DEUTSCHES ELEKTRONEN-SYNCHROTRON

in der HELMHOLTZ-GEMEINSCHAFT

DESY 06-222

December 2006

Longitudinal Wake Field for an Electron Beam Accelerated through a Ultra-High Field Gradient

Gianluca Geloni, Evgeni Saldin, Evgeni Schneidmiller and Mikhail Yurkov

Deutsches Elektronen-Synchrotron DESY, Hamburg

ISSN 0418-9833

NOTKESTRASSE 85 - 22607 HAMBURG

Longitudinal Wake Field for an Electron Beam Accelerated through a Ultra-High Field Gradient

Gianluca Geloni [a] Evgeni Saldin [a] Evgeni Schneidmiller [a]
Mikhail Yurkov [a]

[a] *Deutsches Elektronen-Synchrotron (DESY), Hamburg, Germany*

Abstract

Electron accelerators with higher and higher longitudinal field gradients are desirable, as they allow for the production of high energy beams by means of compact and cheap setups. The new laser-plasma acceleration technique appears to constitute the more promising breakthrough in this direction, delivering unprecedent field gradients up to TV/m. In this article we give a quantitative description of the impact of longitudinal wake fields on the electron beam. Our paper is based on the solution of Maxwell's equations for the longitudinal field. Our conclusions are valid when the acceleration distance is much smaller than the the overtaking length, that is the length that electrons travel as a light signal from the tail of the bunch overtakes the head of the bunch. This condition is well verified for laser-plasma devices. We calculate a closed expression for the impedance and the wake function that may be evaluated numerically. It is shown that the rate of energy loss in the bunch due to radiative interaction is equal to the energy emitted through coherent radiation in the far-zone. Furthermore, an expression is found for the asymptotic limit of a large distance of the electron beam from the accelerator compared with the overtaking length. Such expression allows us to calculate analytical solutions for a Gaussian transverse and longitudinal bunch shape. Finally, we study the feasibility of Table-Top Free-Electron Lasers in the Vacuum Ultra-Violet (TT-VUV FEL) and X-ray range (TT-XFEL), respectively based on 100 MeV and 1 GeV laser-plasma accelerator drivers. Numerical estimations presented in this paper indicate that the effects of the time-dependent energy change induced by the longitudinal wake pose a serious threat to the operation of these devices.

Key words:
Laser-plasma acceleration, longitudinal impedance, longitudinal wake-function, Table-Top X-Ray Free-Electron Laser (TT-XFEL)
PACS: 41.60.Ap, 41.60.-m, 41.20.-q

1 Introduction

The quest for the ultimate electron accelerator will never end. A better beam quality, a higher energy, a smaller size and lower costs will always be goals to be pursued. In particular, size and costs are strictly related. This justifies research activities towards higher and higher longitudinal field gradients. The availability of higher longitudinal field gradients is obviously related, in its turn, to the possibility of production of beams with higher energies.

At the present day, particle accelerator technology is mainly based on Radio-Frequency (RF) devices. However, in the past few years a novel laser-plasma acceleration method has been developed and experimentally demonstrated [1, 2, 3], that promises to outclass all existing accelerator technologies. The laser-plasma acceleration technique requires an ultrashort (a few femtoseconds long) high intensity (Tera to Peta-Watt) laser pulse focused into a supersonic Helium gas jet (or filled capillary) with density around $10^{19}/cm^3$. This produces a region free of electrons propagating behind the laser pulse. Many electrons (up to 10^{10}) are captured in this electron-free zone after about one plasma oscillation, and eventually accelerated by the huge electric field produced by the positive ion background with gradients up to TV/m. Up-to-date experimental verifications demonstrated gradients of the order of 100 GeV/m, that can potentially accelerate electrons up to energies in the GeV-range within a few millimeters.

In this paper we study the important issue of longitudinal wake fields produced within electron beams accelerated with high-gradient fields. We assume that the acceleration distance d_a is much smaller than the the overtaking length. This is the distance travelled by the electrons as a light signal from the tail of the bunch overtakes the head of the bunch. Given a bunch of rms length σ_z, the overtaking length can thus be written as $2\gamma^2\sigma_z$, and corresponds to the radiation formation length $2\gamma^2\lambda\!\!\!^{-}$ calculated at $\lambda\!\!\!^{-} = \sigma_z$, $\lambda\!\!\!^{-} = \lambda/(2\pi)$ being the reduced radiation wavelength. When $d_a \ll 2\gamma^2\sigma_z$, the electrons can be assumed to be accelerated at a single position z_A down the beamline. This is the case for laser-plasma devices, since acceleration in the GeV range takes place within a few millimeters only. However, it is not the case for conventional accelerators, that feature typical gradients up to a few tens of MeV/m, and thus need several tens of meters to reach the GeV range. The assumption $d_a \ll 2\gamma^2\sigma_z$ greatly simplifies wake calculations. In particular, when this condition is verified, the wake generated along the part of the trajectory following the acceleration point z_A is independent of any detail of the particular realization of the accelerator. In this sense, our study is fundamental, because it remains valid independently of the particle accelerator technology chosen, provided that $d_a \ll 2\gamma^2\sigma_z$. One may also have contributions to the wake generated along the part of the

trajectory following the acceleration point z_A. These contributions depend on the physical nature of the accelerator, can be separately calculated, and will be neglected in this paper because they do not affect the bunch in the case of a laser-plasma accelerator.

We base our study on the solution of Maxwell's equations for the longitudinal field. With the help of the fundamental example of an electron travelling in uniform motion we show that the paraxial approximation can be applied to describe electromagnetic sources up to the observation point, while sources after the observation point in the beam propagation direction can be neglected. Then we make use of the paraxial approximation to calculate the Fourier transform of the longitudinal field produced by fixed electromagnetic sources (current and charge densities) at a certain observation plane down the beamline. This expression is at the basis of our treatment, because it allows to calculate a closed expression for the longitudinal impedance and for the wake function to be evaluated numerically. The knowledge of the real part of the impedance further allows verification of the energy conservation principle. Impedance and wake function yield an analytical expression in the asymptotic limit of a large distance of the electron beam from the accelerator compared with the overtaking length, i.e. in the far-field zone for all wavelengths of interest (up to $\lambda\!\!\!^{-} \sim \sigma_z$). This asymptotic limit is of practical relevance, as it allows simple estimations of the impact of the longitudinal wake on the electron beam energy change.

We give an application of our theoretical work by studying the feasibility of Free-electron Lasers (FELs) drivers, proposed as a possible use of laser-plasma accelerators.

Coherent sources of electromagnetic radiation have become very important research tools in science and industry. Recent advance in conventional (RF) particle accelerator techniques allow to construct and operate Free-Electron Lasers in the VUV as well as in the X-ray range. Lasing at wavelengths shorter than the ultra-violet can be achieved with a single-pass, high-gain FEL amplifier. Because of the lack of powerful, coherent seeding sources, short-wavelength FELs work in the so-called Self-Amplified Spontaneous Emission (SASE) mode, where the amplification process starts from shot noise in the electron beam [4, 5, 6]. Experimental realization of SASE FELs developed very rapidly during the last decade. The shortest wavelength ever generated by an FEL, $\lambda = 13$ nm, has been achieved in 2006 at FLASH (Free-electron LAser in Hamburg). Regular user operation of FLASH started in 2005 [7]. Currently, this facility produces GW-level laser-like radiation pulses with 10 to 50 fs duration in the wavelength range from 13 to 45 nm. Recently, the German government, encouraged by these results, approved funding a hard X-ray SASE FEL (XFEL) user facility, the European XFEL [8]. The US department of Energy (DOE) has approved the start of construction

of the Linac Coherent Light Source (LCLS) at the Stanford Linear Accelerator Center (SLAC) [9]. The LCLS and the European XFEL project are scheduled to start operation in 2009 and 2013 respectively.

With the recent progress in the development of laser-plasma accelerators [1, 2, 3] a discussion started about wether and how this technology can be used to provide a cost-effective driver for SASE FELs. The very short length scale of plasma acceleration may eventually allow for the development of very compact laser-like sources both in the VUV and in the X-ray range. In this paper we will not address the delicate issue of technical realization of such table-top FEL drivers. These should finally provide short bunches up to about 10 fs duration in the 100 kA current class (i.e. with a charge of about 1 nC), featuring a relative energy spread of 0.1% for beam energies in the GeV range and a normalized emittance in the order of 1 mm·mrad. Instead, we will restrict our discussion to fundamental electrodynamical questions, supposing that laser-plasma drivers already exist. Once this assumption is made, there are two ways of taking advantage of such device.

The first way is conservative. Up-to-date laser-plasma technology can produce beam energies up to about 1 GeV. With this energy, one may use parameters for the system electron beam-undulator in the same range of those at FLASH. In this fashion one may eventually achieve wavelengths up to $5 \div 10$ nm. This application amounts to substitution of the conventional accelerator system at FLASH with the table-top laser-plasma driver. This would not lead to a table-top VUV-FEL, but it would certainly reduce its size. The only condition for this scheme to work is that a laser-plasma driver capable of providing the same beam parameters as the accelerator system at FLASH must first be built in reality.

The second way is more ambitious, and consists in using laser-plasma accelerators in the GeV range to build Table-Top X-ray FELs by using a completely different set of parameters for the system electron beam-undulator. Namely, an order of magnitude smaller electron energy, an order of magnitude larger peak current, an order of magnitude smaller undulator parameter and an order of magnitude shorter undulator period. The present study allows to estimate the influence of longitudinal wake fields on the relative energy change of the electron beam. In particular, we estimate the magnitude of the induced correlated energy-change as a function of the position within the bunch, as electrons travel through the undulator. This is a fundamental effect that cannot be avoided by fine tuning of the parameters of the setup. Moreover, the energy change grows during the passage of the beam through the undulator, so that one cannot assume a fixed correlated energy change through the undulator. Our conclusion is that the magnitude of this effect poses a serious threat to the feasibility of a table-top FEL in the x-ray range (TT-XFEL), as well as in the VUV range (TT-VUV FEL).

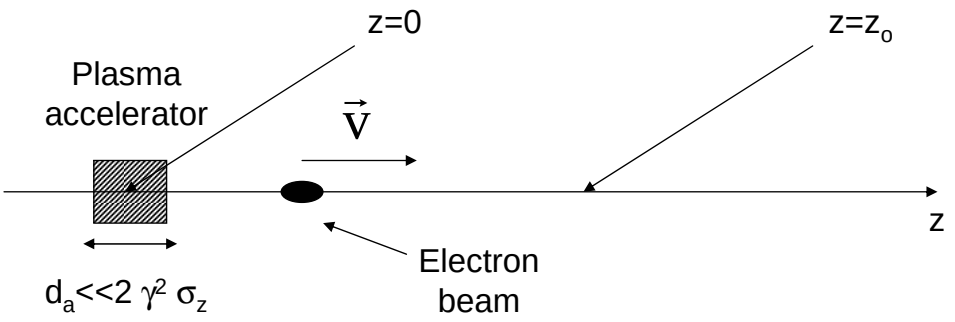

Fig. 1. Geometry.

Our work is organized as follows. First, in Section 2 we calculate the longitudinal field in the space-frequency domain. In the following Section 3 we introduce the basic quantities impedance and wake function, and we review their relation with the Poynting theorem. In Section 4 we present an analytical expression for the asymptotes of the longitudinal impedance in the limit for a large longitudinal distance of the beam with respect to the overtaking length. We further verify the energy conservation principle in Section 5. Section 6 is dedicated to the calculation of an analytical expression for the asymptotes of the longitudinal wake, always in the limit for a large longitudinal distance of the beam with respect to the overtaking length. Finally, our study about the feasibility of the TT-VUV FEL and the TT-XFEL is given in Section 7. Section 8 concludes our work with a few final remarks.

2 Calculation of the longitudinal field in the space-frequency domain

Consider the scheme in Fig. 1, representing the object of our study. Consider position z_A, representing the exit of the plasma accelerator. At this position, the nominal Lorentz factor of electrons is γ. The accelerator switches on both harmonics of the sources and of the field. Since we consider the wake generated along the part of the trajectory following the acceleration point z_A, the nature of the switcher is not important. It is important, though, that the switching process happens on a longitudinal scale $d_a \ll 2\gamma^2 \lambda\!\!\!^{-}$, representing the distance that a light signal has to travel before it overtakes an electron of a distance $\lambda\!\!\!^{-} = c/\omega$, c being the speed of light in vacuum and ω the angular frequency of the radiation in the space-frequency domain. Significant emission of radiation in vacuum is present for wavelengths longer than the longitudinal bunch length σ_z, up to transverse beam sizes $\sigma_\perp \lesssim \gamma\sigma_z$ as we will see. As a result, for typical ultra-relativistic beams the condition

$d_a \ll 2\gamma^2 \lambda$ can be read $d_a \ll 2\gamma^2\sigma_z$, $2\gamma^2\sigma_z$ being the overtaking length.

We begin our investigation with the help of general knowledge of electromagnetic theory [10], by calculating the longitudinal electric field in the space-frequency domain [1] $\bar{E}_z(z_o, \vec{r}_{\perp o}, \omega)$ produced at frequency ω by given electromagnetic sources in vacuum and detected at longitudinal position $z_o > z_A$ and transverse position $\vec{r}_o$ (see Fig. 1).

The field in the space-frequency domain $\vec{\bar{E}}(z_o, \vec{r}_{\perp o}, \omega)$ is the Fourier transform of the field in the space-time domain, $\vec{E}(z_o, \vec{r}_{\perp o}, t)$. As is well-known, for a fixed frequency $\omega = \omega_o$ the field in the space-frequency domain is strictly related to the amplitude $\vec{\bar{E}}_{\omega_o}(z_o, \vec{r}_{\perp o})$ of a monochromatic field oscillating in time with angular frequency ω. In fact

$$\vec{E}(z_o, \vec{r}_{\perp o}, t) = \vec{\bar{E}}_{\omega_o}(z_o, \vec{r}_{\perp o}) \exp\left[-i\omega_o t\right] + C.C. \,, \tag{1}$$

where "C.C." indicates the complex conjugate of the preceding term. It follows that

$$\vec{\bar{E}}(z_o, \vec{r}_{\perp o}, \omega_o) = 2\pi \vec{\bar{E}}_{\omega}(z_o, \vec{r}_{\perp o}) \delta(\omega - \omega_o) \,. \tag{2}$$

Therefore, one may use the field in the space-frequency domain for a given frequency and yet think of the amplitude of a monochromatic field or vicev-

[1] In this paper we define Fourier transform and inverse transform pair of a function $f(t)$ as

$$\bar{f}(\omega) = \int dt \; f(t) \exp\left[i\omega t\right] \; ; \;\; f(t) = \frac{1}{2\pi} \int d\omega \; \bar{f}(\omega) \exp\left[-i\omega t\right] \,.$$

For future use, we also write, explicitly, the definitions of the two-dimensional Fourier transform and inverse transform of a function $g(\vec{r})$ in agreement with the one-dimensional notation:

$$\tilde{g}(\vec{k}) = \int \mathrm{d}\vec{r} \, g(\vec{r}) \exp\left[i\vec{r} \cdot \vec{k}\right] \; ; \;\; g(\vec{r}) = \frac{1}{4\pi^2} \int \mathrm{d}\vec{k} \, \tilde{g}(\vec{k}) \exp\left[-i\vec{r} \cdot \vec{k}\right],$$

the integration being understood over the entire plane. If g is circular symmetric we can introduce the Fourier-Bessel transform and inverse transform pair:

$$\tilde{g}(k) = 2\pi \int_0^\infty dr \; r g(r) J_o(kr) \; ; \;\; g(r) = \frac{1}{2\pi} \int_0^\infty dk \; k \tilde{g}(k) J_o(kr) \,,$$

r and k indicating the modulus of the vectors $\vec{r}$ and $\vec{k}$ respectively, and J_o being the zero-th order Bessel function of the first kind.

ersa. In fact, although they have different dimensions, the knowledge of one quantity fully identifies the other through Eq. (2). As an example, $\vec{\vec{E}}$ satisfies the Helmholtz equation

$$c^2\nabla^2\vec{\vec{E}} + \omega^2\vec{\vec{E}} = 4\pi c^2\vec{\nabla}\bar{\rho} - 4\pi i\omega\vec{\bar{j}}\,, \tag{3}$$

where $\bar{\rho}(\vec{r},\omega)$ and $\vec{\bar{j}}(\vec{r},\omega)$ are the Fourier transforms of the space-time domain charge density $\rho(\vec{r},t)$ and current density $\vec{j}(\vec{r},t)$. In the same way, an equation for $\vec{\vec{E}}_\omega$ is found substituting $\vec{\bar{j}}$ and ρ with $\vec{\bar{j}}_\omega$ and ρ_ω, related to $\vec{\bar{j}}$ and $\bar{\rho}$ through an analogous of Eq. (2).

Eq. (3) can be solved with the help of an appropriate Green's function $G(z_o - z', \vec{r}_{\perp o} - \vec{r'}_\perp)$ yielding

$$\bar{E}_z(z_o,\vec{r}_{\perp o},\omega) = -4\pi\int_{-\infty}^{\infty} dz'\int d\vec{r'}_\perp\left(\frac{i\omega}{c^2}\bar{j}_z - \frac{\partial\bar{\rho}}{\partial z'}\right)G(z_o - z', \vec{r}_{\perp o} - \vec{r'}_\perp)\,, \tag{4}$$

the integration in $d\vec{r'}_\perp$ being performed over the entire transverse plane. An explicit expression for the Green's function to be used in Eq. (4) is given by

$$G(z_o - z', \vec{r}_{\perp o} - \vec{r'}_\perp) = -\frac{\exp\left\{i(\omega/c)\left[\left|\vec{r}_{\perp o} - \vec{r'}_\perp\right|^2 + (z_o - z')^2\right]^{1/2}\right\}}{4\pi\left[\left|\vec{r}_{\perp o} - \vec{r'}_\perp\right|^2 + (z_o - z')^2\right]^{1/2}}\,, \tag{5}$$

that automatically includes the proper boundary conditions at infinity.

Since electrons are moving along the z-axis, we write the harmonic components of the charge and current density, $\bar{\rho}$ and $\bar{j}_z$ as

$$\bar{\rho}\left(z', \vec{r'}_\perp, \omega\right) = \rho_o\left(\vec{r'}_\perp\right)\bar{f}(\omega)\exp\left[i\frac{\omega z'}{v}\right]u(z' - z_A) \tag{6}$$

and

$$\bar{j}_z\left(z', \vec{r'}_\perp, \omega\right) = \beta c\bar{\rho}\,. \tag{7}$$

Notation $u(z' - z_A)$ in Eq. (6) indicates a Heaviside step function centered at position z_A, whose presence signifies that there are no sources before the plasma accelerator, i.e. before the point $z' = z_A$. This describes a switch-on

process. When the switching distance $d \ll 2\gamma^2\sigma_z$, the nature of the switcher is not important for the description of the wake associated with Eq. (6) and Eq. (7), i.e. the wake generated along the part of the trajectory following the acceleration point z_A. However, Eq. (6) and Eq. (7) alone violate the continuity equation, and should be completed by extra-contributions that depend on the nature of the switcher. For example, if one thinks of an acceleration process where a low energy bunch with Lorentz factor γ_o is accelerated on a distance d up to a Lorentz factor γ, one should add to Eq. (6) and Eq. (7) the contribution of the harmonic at frequency ω associated with the beam with Lorentz factor γ_o. Such harmonic is characterized by a different longitudinal velocity $\beta_o c$ with respect to βc, and by a different wave number $k_o = \omega/v_o$. However, its amplitude is the same of that after the acceleration process:

$$\bar{\rho}_o\left(z', \vec{r'}_\perp, \omega\right) = \rho_o\left(\vec{r'}_\perp\right) \bar{f}(\omega) \exp\left[i\frac{\omega z'}{v_o}\right] [1 - u(z' - z_A)] \tag{8}$$

and

$$\bar{j}_{oz}\left(z', \vec{r'}_\perp, \omega\right) = \beta_o c \bar{\rho} \, . \tag{9}$$

As a result, the continuity equation is satisfied. However, Eq. (8) and Eq. (9) depend on the particular process described (acceleration from v_o to v), so that their contribution depends on the particular switching process selected. In this paper we will not consider this contribution. We will focus, instead, on the switch-independent part of the problem. Note that for the case of a plasma accelerator, Eq. (8) and Eq. (9) should be replaced by contributions due to a positive ion current propagating in the opposite direction with respect to the electrons. As a result we can neglect such source, that has no effect on the longitudinal wake field acting on the electron beam.

The assumption of separability of variables z' and $\vec{r'}_\perp$, in Eq. (6), together with the fact that the function $\bar{f}$ is independent of z' may be satisfied as long as the transverse electron beam size $\sigma_\perp$ remains unvaried along a formation length. This happens for an angular divergence σ_θ such that $\sigma_\perp \gg \sigma_\theta \gamma^2 \sigma_z$. Moreover, the assumption of separability also requires that we can neglect dynamical effects of self-interactions, because there is no external force acting on the bunch. In this sense, we are developing the zero-th order treatment of a perturbation theory, where the perturbation to the particles dynamics is given by the self-interaction within the electron bunch. The quantity ρ_o has the meaning of transverse electron beam distribution; in principle, it may depend on the harmonic ω, but in the following we will assume it does not. Thus, all information about the longitudinal electron density distribution $f(t)$ is included in the function $\bar{f}(\omega)$, that is its Fourier

transform. A typical Gaussian beam model, that will be useful later on, is defined by

$$\rho_o\left(\vec{r'}_\perp\right) = \frac{1}{2\pi\sigma_\perp^2 c}\exp\left[-\frac{r_\perp'^2}{2\sigma_\perp^2}\right], \tag{10}$$

$\sigma_\perp$ being the *rms* beam transverse dimension and by

$$f(t) = \frac{(-e)N}{\sqrt{2\pi}\sigma_t}\exp\left[-\frac{t^2}{2\sigma_t^2}\right] \quad \longleftrightarrow \quad \bar{f}(\omega) = (-e)N\exp\left[-\frac{\omega^2\sigma_t^2}{2}\right], \tag{11}$$

where N is the number of electrons in the beam and $(-e)$ the electron beam charge. Moreover, σ_t is the *rms* bunch duration, connected with the *rms* bunch length by $\sigma_z = \beta c\sigma_t$, so that in terms of lengths

$$f(s) = \frac{(-e)N}{\sqrt{2\pi}\sigma_z}\exp\left[-\frac{s^2}{2\sigma_z^2}\right]. \tag{12}$$

We now account for Eq. (6) and Eq. (7) and calculate the derivative of $\bar{\rho}$ with respect to z' in Eq. (4), but keep the implicit form for G. We obtain

$$\begin{aligned}\bar{E}_z = \frac{4\pi i\omega\bar{f}(\omega)}{\gamma^2 c}\int d\vec{r'}_\perp\rho_o\left(\vec{r'}_\perp\right)\int_{z_A}^{\infty}dz'\exp\left[i\frac{\omega z'}{v}\right]G(z_o - z', \vec{r}_{\perp o} - \vec{r'}_\perp)\\ +4\pi\bar{f}(\omega)\exp\left[i\frac{\omega z_A}{v}\right]\int d\vec{r'}_\perp\rho_o\left(\vec{r'}_\perp\right)G(z_o - z_A, \vec{r}_{\perp o} - \vec{r'}_\perp).\end{aligned} \tag{13}$$

The integration domain in dz' in Eq. (13), that is $[z_A, \infty)$, can be represented as $[z_A, z_o]\cup[z_o, \infty)$. The integral in dz' can be written as the sum of two integrals in dz' performed over the separate domains $[z_A, z_o]$ and $[z_o, \infty)$. At this point we perform the following operations. First, we neglect the integral over the interval $[z_o, \infty)$, i.e. we neglect the effects of electromagnetic sources located in $[z_o, \infty)$. Second, we apply the paraxial approximation. This means that we solve, for sources located in $[z_A, z_o]$, the paraxial equation

$$c^2\exp\left[i\frac{\omega}{c}z\right]\left(\nabla_\perp^2 + \frac{2i\omega}{c}\frac{\partial}{\partial z}\right)\vec{\tilde{E}} = 4\pi c^2\vec{\nabla}\bar{\rho} - 4\pi i\omega\vec{\tilde{j}}, \tag{14}$$

where we introduced the envelope of the field components

$$\vec{\tilde{E}} = \vec{\bar{E}}\exp\left[-i\omega z/c\right], \tag{15}$$

because paraxial approximation implies a slowly varying envelope of the field with respect to the wavelength $\lambda = 2\pi c/\omega$. Note that the source term of Eq. (14) is now multiplied by a phase factor $\exp[-i\omega z/c]$ with respect to that of Helmholtz equation, Eq. (3). As a result, we can obtain an expression for $\widetilde{E}_z$ by formally operating in Eq. (13) in the following way. First, we restrict the integration limits in dz' to $[z_A, z_o]$. Second, we substitute the Green's function G with $\exp[-i\omega z/c] \cdot G_p$, where G_p is the Green's function for the paraxial equation:

$$G_p(z_o - z', \vec{r}_{\perp o} - \vec{r'}_\perp) = -\frac{1}{4\pi(z_o - z')} \exp\left[i\omega \frac{|\,\vec{r}_{\perp o} - \vec{r'}_\perp\,|^2}{2c(z_o - z')}\right] . \tag{16}$$

We then obtain the following expression for $\widetilde{E}_z$:

$$\begin{aligned}
&\widetilde{E}_z(z_o, \vec{r}_{\perp o}, \omega) = \\
&-\frac{i\omega \bar{f}(\omega)}{\gamma^2 c} \int d\vec{r'}_\perp \rho_o\left(\vec{r'}_\perp\right) \int_{z_A}^{z_o} \frac{dz'}{(z_o - z')} \exp\left[\frac{i\omega z'}{2\gamma^2 c} + i\omega \frac{|\,\vec{r}_{\perp o} - \vec{r'}_\perp\,|^2}{2c(z_o - z')}\right] \\
&-\frac{\bar{f}(\omega)}{(z_o - z_A)} \exp\left[\frac{i\omega z_A}{2\gamma^2 c}\right] \int d\vec{r'}_\perp \rho_o\left(\vec{r'}_\perp\right) \exp\left[i\omega \frac{|\,\vec{r}_{\perp o} - \vec{r'}_\perp\,|^2}{2c(z_o - z_A)}\right] ,
\end{aligned} \tag{17}$$

We do not present here a general proof of the validity of Eq. (17). We rather verify its correctness in the particular case $z_A \longrightarrow -\infty, z_o = 0, \rho_o\left(\vec{r'}_\perp\right) = \delta\left(\vec{r'}_\perp\right)$ and $\bar{f}(\omega) = (-e)$. This corresponds to Fourier transform of the field of a particle in uniform motion, calculated at position $(0, \vec{r}_{\perp o})$. In the chosen limit, Eq. (17) becomes

$$\widetilde{E}_z(0, r_{\perp o}, \omega) = \frac{i\omega(-e)}{\gamma^2 c} \int_{-\infty}^{0} dz' \frac{1}{z'} \exp\left[\frac{i\omega z'}{2\gamma^2 c} - i\omega \frac{r_{\perp o}^2}{2cz'}\right] , \tag{18}$$

depending on the modulus of $\vec{r}_{\perp o}$ only. The integral in Eq. (18) can be performed analytically using $-\omega z'/(2\gamma^2 c)$ as integration variable in place of z' and taking advantage of the following relation, that is valid for values $\alpha > 0$:

$$\int_0^\infty \frac{dx}{x} \exp\left[i\left(-x + \frac{\alpha}{x}\right)\right] = 2\int_0^\infty d\xi \frac{\cos\left(2\sqrt{\alpha}\xi\right)}{\sqrt{1 + \xi^2}} = 2K_o\left(2\sqrt{\alpha}\right) , \tag{19}$$

where K_n indicates the n-th order modified Bessel function of the second kind. We thus obtain the following expression:

$$\widetilde{E}_z(0, r_{\perp o}, \omega) = -\frac{2i\omega(-e)}{\gamma^2 c} K_o\left(\frac{\omega r_{\perp o}}{c\gamma}\right) , \tag{20}$$

in perfect agreement (aside for notational differences) with Eq. (13.80) of [10], following directly from the Fourier transform of the time-domain electric field.

To conclude this Section, we give an explicit presentation of Eq. (17) in the case $z_A \longrightarrow -\infty$, that corresponds to the steady state solution for the electric field, and for $z_A = 0$, that represents the switch-on case without loss of generality.

In the case $z_A \longrightarrow -\infty$ we can make still take advantage of Eq. (19). Then, in the steady state limit, Eq. (17) becomes

$$\widetilde{E}_z\ (z_o, \vec{r}_{\perp o}, \omega) = -\frac{2i\omega}{\gamma^2 c} \exp\left[\frac{i\omega z_o}{2\gamma^2 c}\right] \bar{f}(\omega) \int d\vec{r'}_\perp\ \rho_o(\vec{r'}_\perp) K_o\left(\frac{\omega\ |\ \vec{r}_{\perp o} - \vec{r'}_\perp\ |}{\gamma c}\right) . \tag{21}$$

It should be noted that in this case, the dependence of $\widetilde{E}_z$ on z_o is restricted to a phase factor only (steady state solution). In the case $z_A = 0$, direct substitution in Eq. (17) yields

$$\begin{aligned} \widetilde{E}_z(z_o, \vec{r}_{\perp o}, \omega) &= -\frac{\omega \bar{f}(\omega)}{\gamma^2 c} \int d\vec{r'}_\perp \rho_o\left(\vec{r'}_\perp\right) \\ &\times \left\{ i \int_0^{z_o} \frac{dz'}{(z_o - z')} \exp\left[\frac{i\omega z'}{2\gamma^2 c} + i\omega \frac{|\ \vec{r}_{\perp o} - \vec{r'}_\perp\ |^2}{2c(z_o - z')}\right] + \frac{\gamma^2 c}{\omega z_o} \exp\left[i\omega \frac{|\ \vec{r}_{\perp o} - \vec{r'}_\perp\ |^2}{2cz_o}\right] \right\} , \end{aligned} \tag{22}$$

It can be verified by inspection that, in the limit for $z_o \gg 2\gamma^2 \lambda\!\!\!^{-}$, Eq. (22) gives back the steady state solution, Eq. (21). Eq. (21) and Eq. (22) or, more in general, Eq. (17) can now be used to estimate the impact of the field generated by the electron beam on any particle in the beam. We do so with the help of the concepts of wake fields and impedances, that are related to the Poynting theorem as reviewed in the following Section.

3 Poynting theorem in the frequency domain, longitudinal wake fields and impedances

In the time domain, the Poynting theorem [10] reads, at any time t:

$$\int_V \vec{j} \cdot \vec{E}\, dV + \int_A \vec{S} \cdot \hat{n}\, dA + \frac{d}{dt} \int_V (w_e - w_m)\, dV = 0\,. \tag{23}$$

Notations V and A in Eq. (23) respectively indicate any finite volume and its surrounding surface, while $\hat{n}$ denotes the field of unit vectors normal to A, directed outwards. In this way, the second integral in Eq. (23) represents the flux of the Poynting vector, while the first and the second integrals are volume integrals calculated within V. In Eq. (23) we introduced the Poynting vector $\vec{S}$ and the energy densities w_e and w_m, understanding that they all are functions of time, in the following way:

$$\vec{S} = \frac{c}{4\pi}\left(\vec{E} \times \vec{B}\right)\,, \quad w_e = \frac{1}{8\pi}\left|\vec{E}\right|^2 \text{ and } w_m = \frac{1}{8\pi}\left|\vec{B}\right|^2\,. \tag{24}$$

Eq. (23) is an exact identity following from Maxwell's equations in the time domain. Quantities in Eq. (23) have the dimension of [energy]/[time].

As is well-known [10], a version of the Poynting theorem in the space-frequency domain can be derived starting with the Poynting theorem in the space-time domain formulated for a monochromatic field like in Eq. (1) and averaging over a cycle of oscillation in time. Then, use of Eq. (2) yields the following complex relation for space-frequency domain quantities:

$$2\int_V \vec{\bar{j}}^{\,*} \cdot \vec{\bar{E}}\, dV + \int_A \vec{\bar{S}} \cdot \hat{n}\, dA + i\omega \int_V (\bar{w}_e - \bar{w}_m)\, dV = 0\,. \tag{25}$$

Here we define the complex, space-frequency domain version of the Poynting vector $\vec{\bar{S}}$ and of the electric $\bar{w}_e$ and magnetic $\bar{w}_m$ energy densities in vacuum as

$$\vec{\bar{S}} = \frac{c}{2\pi}\left(\vec{\bar{E}} \times \vec{\bar{B}}^{\,*}\right)\,, \quad \bar{w}_e = \frac{1}{4\pi}\left|\vec{\bar{E}}\right|^2 \text{ and } \bar{w}_m = \frac{1}{4\pi}\left|\vec{\bar{B}}\right|^2\,. \tag{26}$$

Eq. (25) is an exact identity following from Maxwell's equations in the frequency domain. Note that now quantities in Eq. (25) have the dimension of [energy]/[frequency], i.e. of a spectral energy density integrated through a given surface. In our case, we can separately write real and imaginary parts of Eq. (25) as

$$2\int_V \mathrm{Re}\left[\vec{\bar{j}}^{\,*} \cdot \vec{\bar{E}}\right] dV + \int_A \mathrm{Re}\left[\vec{\bar{S}} \cdot \hat{n}\right] dA = 0\,. \tag{27}$$

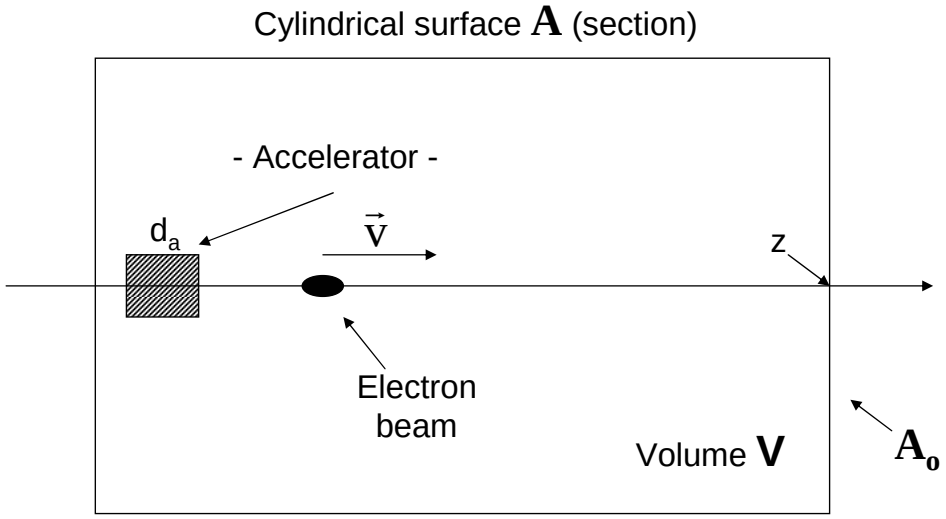

Fig. 2. Geometry for application of Poynting theorem.

and

$$2\int_V \mathrm{Im}\left[\vec{\bar{j}}^{\,*}\cdot\vec{\bar{E}}\right]\,dV+\omega\int_V(\bar{w}_e-\bar{w}_m)\,dV+\int_A \mathrm{Im}\left[\vec{\bar{S}}\cdot\hat{n}\right]\,dA=0\,. \qquad (28)$$

Eq. (27) expresses energy conservation of time-averaged quantities, while Eq. (28) ”relates to the reactive or stored energy and its alternating flow” (cited from [10]). In our case we consider the volume V and the surface A of cylindrical shape as depicted in Fig. 2. From Eq. (27) follows the equality between the total energy losses of the whole bunch and the energy of coherent radiation in the far zone, a fact that we will verify later on. Since $\vec{\bar{j}}$ is directed longitudinally we can write such equality (always with reference to Fig. 2) as

$$2\int_V \mathrm{Re}\left[\bar{j}_z^{\,*}\bar{E}_z\right]\,dV=-\frac{c}{2\pi}\int_{A_o}\left|\vec{\bar{E}}_\perp\right|^2\,dA\,, \qquad (29)$$

where $\vec{\bar{E}}_\perp$ indicates the radiation field. The volume integral of the quantity $2\bar{j}_z^{\,*}\bar{E}_z$ can be explicitly written with the help of Eq. (22) and Eq. (7) as

$$2\int_V \bar{j}_z^{\,*}\bar{E}_z\,dV=\left|\bar{f}(\omega)\right|^2 X(\omega) \qquad (30)$$

where

$$X(\omega) = -\frac{2\omega}{\gamma^2}\int d\vec{r'}_\perp \int d\vec{r''}_\perp \rho_o^*(\vec{r'}_\perp)\rho_o(\vec{r''}_\perp)\int_0^z dz' \times\left\{ i\int_0^{z'} \frac{dz''}{(z'-z'')}\exp\left[\frac{i\omega(z''-z')}{2\gamma^2 c} + i\omega\frac{|\,\vec{r}_{\perp o}-\vec{r'}_\perp\,|^2}{2c(z'-z'')}\right] + \frac{\gamma^2 c}{\omega z'}\exp\left[i\omega\frac{|\,\vec{r}_{\perp o}-\vec{r'}_\perp\,|^2}{2cz'}\right]\exp\left[-\frac{i\omega z'}{2\gamma^2 c}\right]\right\}. \tag{31}$$

Note that that ρ_o is a real quantity. The quantity $X(\omega)$ has the property $X(\omega) = X^*(-\omega)$, as it can be directly verified. This means that Re$[X](\omega)$ is an even function of ω, while Im$[X](\omega)$ is odd. $X(\omega)$ is strictly related to $\Delta E_{\rm tot}$, the total energy lost by the bunch as it travels within the volume V. In fact, $\Delta E_{\rm tot}$ is given by

$$\Delta\mathcal{E}_{\rm tot} = \frac{c}{4\pi}\int_{A_o} dA \int_{-\infty}^{\infty} dt\left|\vec{E}(t)\right|^2 = \frac{c}{8\pi^2}\int_{A_o} dA\int_{-\infty}^{\infty} d\omega\left|\vec{\tilde{E}}_\perp\right|^2 . \tag{32}$$

Comparison with Eq. (29) yields

$$\Delta\mathcal{E}_{\rm tot} = \frac{1}{2\pi}\int_{-\infty}^{\infty} d\omega\int_V {\rm Re}\left[\bar{j}_z^*\bar{E}_z\right]\, dV = \frac{1}{4\pi}\int_{-\infty}^{\infty} d\omega\left|\bar{f}(\omega)\right|^2 X(\omega)\,. \tag{33}$$

Since $|\bar{f}|^2$ is even, Re$[X](\omega)$ is even, and Im$[X](\omega)$ is odd, we conclude that $\Delta\mathcal{E}_{\rm tot}$ is a positive real quantity, as it must be.

As we will briefly review here, $X(\omega)$ is also strictly related to the impedance of the system. When the bunch is ultra relativistic, the longitudinal impedance of the system, $Z_o(\omega)$ is typically given as the Fourier transform of the wake function $G_o(\Delta s)$, that is

$$Z_o(\omega) = \int_{-\infty}^{\infty}\frac{d(\Delta s)}{\beta c}\,G_o(\Delta s)\exp\left[i\omega\frac{\Delta s}{\beta c}\right], \tag{34}$$

where the wake function is defined as

$$G_o(\Delta s) = \frac{1}{(-e)} \int_{-\infty}^{\infty} dz' \; E_z(\Delta s, t)|_{t=z'/(\beta c)} \; . \tag{35}$$

Here $E_z(\Delta s, t)$ indicates the longitudinal component of the time-domain electric field generated by a source particle acting on a test particle at longitudinal distance Δs from the source. This field is integrated along the test particle trajectory, and divided by the electron charge $(-e)$, so that $e^2 G_o(\Delta s)$ is the energy (gained, or lost) by the test particle due to the action of the source. In agreement with [11] we take the test particle behind the source for positive values of Δs. According to the given definition of wake function, one should integrate the longitudinal field over the entire trajectory. However, there is no principle difficulty in considering only part of the trajectory, let us say, up to position z. Mathematically, this means that the upper integration limit in Eq. (35), i.e. ∞, should be substituted with z. In this way, $G = G(\Delta s, z)$. Moreover, our trajectory is supposed to start at $z_A = 0$, that allows one to substitute the lower integration limit in Eq. (35), i.e. $-\infty$, with 0. We thus obtain

$$G_o(\Delta s, z) = \frac{1}{(-e)} \int_{0}^{z} dz' \; E_z(\Delta s, t)|_{t=z'/(\beta c)} \; . \tag{36}$$

In both Eq. (34) and Eq. (36) we considered a case when test and source particles move along the longitudinal z axis. More in general, we should include given transverse offsets of test and source with respect to the z axis. Therefore we have to modify Eq. (34) and Eq. (36) to include a dependence on such offset, i.e. on the test and source transverse coordinates $\vec{r}_{\perp T}$ and $\vec{r}_{\perp S}$: in this way $G_o = G_o(\Delta s, z, \vec{r}_{\perp S}, \vec{r}_{\perp T})$. In order to make our definitions independent of $\vec{r}_{\perp T}$ and $\vec{r}_{\perp S}$, we integrate over the transverse particle distribution in $d\vec{r}_{\perp T}$ and $d\vec{r}_{\perp S}$. This can be interpreted as a substitution of test and source particles with disks of charge longitudinally separated by a distance Δs. We thus obtain

$$G(\Delta s, z) = \frac{1}{e^2} \int d\vec{r'}_{\perp} \int d\vec{r''}_{\perp} \rho_o(\vec{r'}_{\perp}) \rho_o(\vec{r''}_{\perp}) G_o(\Delta s, z, \vec{r'}_{\perp}, \vec{r''}_{\perp}) \; . \tag{37}$$

In Eq. (37) we used the fact that ρ_o is independent of the longitudinal position. With the redefinition in Eq. (37) we can further consider the impedance $Z(\omega, z)$:

$$Z(\omega, z) = \int_{-\infty}^{\infty} \frac{d(\Delta s)}{\beta c} \; G(\Delta s, z) \exp\left[i\omega \frac{\Delta s}{\beta c} \right] \; . \tag{38}$$

As is well-known, since $G(\Delta s, z)$ is a real function one has $Z(\omega, z) = Z^*(-\omega, z)$, i.e. the impedance has even real part and odd imaginary part. Thus, if we split the wake function in the sum $G = G_S + G_A$ of a symmetric and antisymmetric part, the Fourier transform of G_S gives back Re[Z], while the Fourier Transform of G_A yields Im[Z]. The symmetric part of the wake, G_S, is also called the active part and is related with the energy lost by the bunch through radiation. The antisymmetric part G_A instead, is called the reactive part and is related with energy redistribution within the bunch, but not with the energy radiated. This can be seen by writing the total energy lost by the bunch in terms of $G(\tau)$, where $\tau = s/(\beta c)$:

$$\Delta\mathcal{E}_{\rm tot}(z) = \int_{-\infty}^{\infty} dt \int_{-\infty}^{\infty} d\tau\ G(\tau, z) f(t) f(t-\tau) = \int_{-\infty}^{\infty} d\tau\ G(\tau, z) \mathcal{A}[f](\tau)\ , \tag{39}$$

where $\mathcal{A}[f](\tau)$ indicates the autocorrelation function of f. Since $\mathcal{A}[f](\tau)$ is even in τ, only the symmetric part G_S enters effectively in the expression for $\Delta\mathcal{E}_{\rm tot}$. Finally, using the relation

$$\int_{-\infty}^{\infty} dt g_1(t) g_2^*(t) = \frac{1}{2\pi} \int_{-\infty}^{\infty} d\omega \bar{g}_1(\omega) \bar{g}_2^*(\omega) \tag{40}$$

to simplify Eq. (39) we can write

$$\Delta\mathcal{E}_{\rm tot}(z) = \frac{1}{2\pi} \int_{-\infty}^{\infty} d\omega\ Z(\omega, z) \left|\bar{f}(\omega)\right|^2\ , \tag{41}$$

where we used the autocorrelation theorem to find $\overline{\mathcal{A}[f]} = |\bar{f}|^2 = (\ \overline{\mathcal{A}[f]}\ )^*$ and Eq. (38). In the case $|f(\omega)|^2 = e^2$ (single electron), by definition of impedance, Eq. (34), we have

$$Z(\omega, z) = \frac{1}{e^2} \int_V \bar{j}_z^* \bar{E}_z\, dV \tag{42}$$

and from Eq. (30) we have

$$Z(\omega, z) = \frac{1}{2} X(\omega, z)\ , \tag{43}$$

that yields a practical algorithm to compute both real and imaginary parts of the impedance (and, subsequently, of the wake), through the evaluation of Eq. (31).

Finally, a word of caution. The impedance formalism is often used in order to describe coupling impedances. A typical situation is the following. A given electron in a bunch induces charge and current densities in the vacuum chamber walls. In turn, these charge and current densities are responsible for spurious electromagnetic fields acting back on electrons following the exciting one, thus generating a coupling wake function (and thus its related coupling impedance). This coupling wake function G_c must vanish in front of an exciting particle in the limit for $\gamma \longrightarrow \infty$, i.e. for electron velocities $v \longrightarrow c$. As a result one can take $G_c(\Delta s) = 0$ for $\Delta s < 0$ (see [11]). This property is necessary (although not sufficient) to demonstrate that the coupling impedance Z_c (i.e. the Fourier transform of G_c), obeys the well-known Kramers-Kronig relation [12, 13], thus providing a link between real and imaginary parts of the impedance. However, our impedance does not obey Kramers-Kronig relations. In fact, we are dealing with a mechanism of generation of the wake function that is fundamentally different from that of coupling wakes. In particular $G(\Delta s)$ can be different from zero both for $\Delta s < 0$ and $\Delta s > 0$, a result of the fact that we are dealing both with tail-head as well as with head-tail interactions in the time domain [2].

4 Analytical asymptotes of the longitudinal impedance

Let us write an explicit expression for the impedance with the help of Eq. (31):

$$Z(\omega, z) = Z_1(\omega, z) + Z_2(\omega, z) \, . \tag{44}$$

Here we have defined, for computational convenience, the quantities

$$Z_1(\omega, z) = -\frac{i\omega}{\gamma^2} \int d\vec{r'}_\perp \int d\vec{r''}_\perp \rho_o^*(\vec{r'}_\perp) \rho_o(\vec{r''}_\perp) \times \int_0^z dz' \int_0^{z'} \frac{dz''}{(z' - z'')} \exp\left[\frac{i\omega(z'' - z')}{2\gamma^2 c} + i\omega \frac{|\, \vec{r'}_\perp - \vec{r''}_\perp \,|^2}{2c(z' - z'')} \right] , \tag{45}$$

[2] Note that causality with respect to time remains obviously valid but it cannot be exploited, as in the case of coupling wakes, giving a relation between real and imaginary part of the impedance.

and

$$Z_2(\omega, z) = -\int d\vec{r'}_\perp \int d\vec{r''}_\perp \rho_o^*(\vec{r'}_\perp)\rho_o(\vec{r''}_\perp) \times \int_0^z dz' \frac{c}{z'} \exp\left[i\omega \frac{|\,\vec{r'}_\perp - \vec{r''}_\perp\,|^2}{2cz'}\right] \exp\left[-\frac{i\omega z'}{2\gamma^2 c}\right], \quad (46)$$

Aside for particular cases, the task of calculating real and imaginary part of the impedance must be performed numerically. It is possible, however, to obtain important analytical information about the impedance and wake function in the asymptotic case $z \gg 2\gamma^2 \lambda\!\!\!^{-}$ from Eq. (44).

4.1 Real part

Let us consider Re[Z] for $z \gg 2\gamma^2 \lambda\!\!\!^{-}$. We first deal with Z_2. With the help of Eq. (19), it can be shown that in the limit for $z \gg 2\gamma^2 \lambda\!\!\!^{-}$, Z_2 tends to a real quantity independent of z:

$$Z_2(\omega) = -2c \int d\vec{r'}_\perp \int d\vec{r''}_\perp \rho_o^*(\vec{r'}_\perp)\rho_o(\vec{r''}_\perp) K_o\left(\frac{\omega\,|\,\vec{r'}_\perp - \vec{r''}_\perp\,|}{\gamma c}\right). \quad (47)$$

The integral in $d\vec{r''}_\perp$ can be interpreted as a convolution product between two functions of $\vec{r}_\perp$, i.e. ρ_o and K_o. This is equal to the anti-Fourier transform in two dimensions of the product of the spatial Fourier transforms of ρ_o and K_o, that we will call respectively $\tilde{\rho}_o(\vec{k})$ and $\tilde{K}_o(\vec{k})$, $\vec{k}$ being the conjugate variable to $\vec{r}_\perp$. By exchanging the integration in $d\vec{k}$ and that in $d\vec{r'}_\perp$ one obtains the following alternative representation of Z_2:

$$Z_2(\omega) = -\frac{c}{2\pi^2} \int d\vec{k} \left|\tilde{\rho}_o(\vec{k})\right|^2 \tilde{K}_o\left(\vec{k}\right). \quad (48)$$

As concerns Z_1 we make use of the two identities

$$\frac{2\pi i c}{\omega} \frac{z'z''}{z'-z''} \exp\left[-\frac{i\omega|\vec{r'}_\perp - \vec{r''}_\perp|^2}{2c(z'-z'')}\right] = \int d\vec{r}_\perp \exp\left[-\frac{i\omega|\vec{r}_\perp - \vec{r'}_\perp|^2}{2cz'} + \frac{i\omega|\vec{r}_\perp - \vec{r''}_\perp|^2}{2cz''}\right] \quad (49)$$

and

$$\int_0^z g(z')\,dz' \int_0^{z'} g^*(z'')\,dz'' + C.C. = \left| \int_0^z g(z)\,dz \right|^2 , \tag{50}$$

and of Eq. (19). With the help of these relations we rewrite the real part of Z_1 in the limit for $z \gg 2\gamma^2 \lambda\!\!\!^{-}$ as an expression independent of z:

$$\mathrm{Re}[Z_1](\omega) = \frac{\omega^2}{\pi\gamma^2 c} \int d\vec{r}_\perp \left| \int d\vec{r'}_\perp \rho_o(\vec{r'}_\perp) K_o\left(\frac{\omega \mid \vec{r}_\perp - \vec{r'}_\perp \mid}{\gamma c} \right) \right|^2 . \tag{51}$$

Applying Eq. (40) with $g_1 = g_2$ to Eq. (51) and remembering that the spatial Fourier transform of the convolution product of two function is equal to the product of the spatial Fourier transform of the same function, we can rewrite Eq. (51) as

$$\mathrm{Re}[Z_1](\omega) = \frac{\omega^2}{4\pi^3\gamma^2} \int d\vec{k} \left| \tilde{\rho}_o(\vec{k}) \tilde{K}_o\left(\vec{k}\right) \right|^2 . \tag{52}$$

Thus, putting together Eq. (48) and Eq. (52) we obtain

$$\mathrm{Re}[Z](\omega) = \frac{\omega^2}{4\pi^3\gamma^2} \int d\vec{k} \left| \tilde{\rho}_o(\vec{k}) \tilde{K}_o\left(\vec{k}\right) \right|^2 - \frac{c}{2\pi^2} \int d\vec{k} \left| \tilde{\rho}_o(\vec{k}) \right|^2 \tilde{K}_o\left(\vec{k}\right) . \tag{53}$$

Substitution in Eq. (53) of the explicit expression for $\tilde{K}_o(\vec{k})$

$$\begin{aligned} \tilde{K}_o\left(\vec{k}\right) &= \int d\vec{r}_\perp \exp\left[i\vec{k} \cdot \vec{r}_\perp \right] K_o\left(\frac{\omega \left| \vec{r}_\perp \right|}{\gamma c} \right) = 2\pi \int_0^\infty dr_\perp r_\perp K_o\left(\frac{\omega r_\perp}{\gamma c} \right) J_o(k r_\perp) \\ &= \frac{2\pi c^2 \gamma^2}{\omega^2} \frac{1}{\left[1 + (c\gamma k/\omega)^2 \right]} , \end{aligned} \tag{54}$$

together with the new notation $\vec{\theta} = c\vec{k}/\omega$ yields for the sum of two integrals in Eq. (53):

$$\mathrm{Re}[Z](\omega) = -\frac{c}{\pi} \int d\vec{\theta} \left| \tilde{\rho}_o(\vec{\theta}, \omega) \right|^2 \frac{\gamma^4 \theta^2}{\left(1 + \gamma^2 \theta^2\right)^2} . \tag{55}$$

Up to now we did not make use of any particular model for the electron beam. Choosing Eq. (10) as a model for ρ_o we can substitute into Eq. (55) the following expression for $\tilde{\rho}_o$:

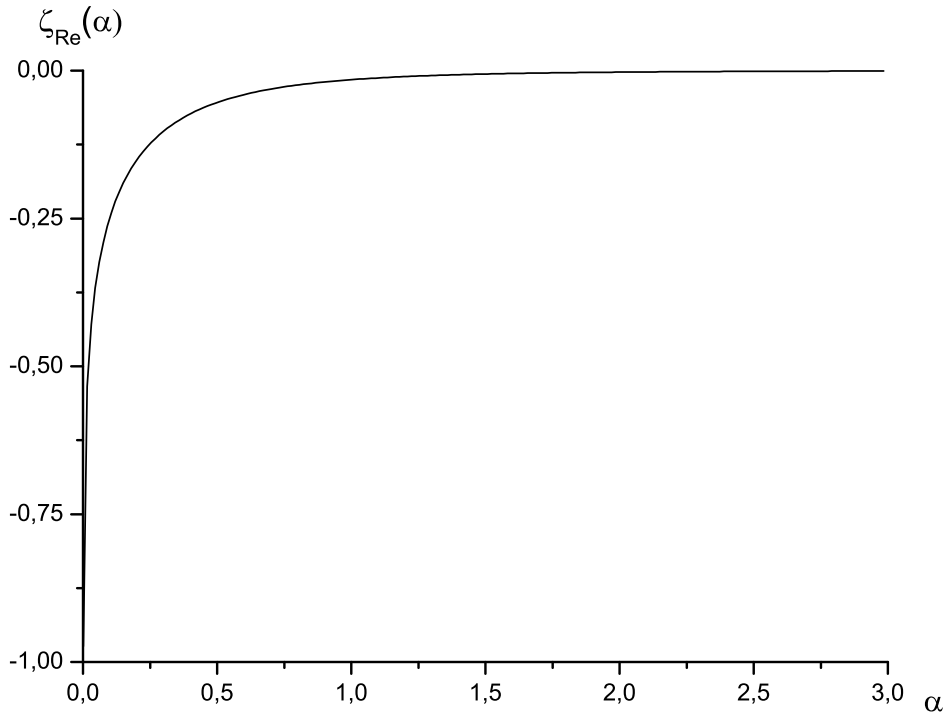

Fig. 3. Plot of the universal function ζ_{Re}, as a function of α.

$$\tilde{\rho}_o\left(\vec{\theta},\omega\right) = \frac{1}{c}\exp\left[-\frac{\theta^2\omega^2\sigma_\perp^2}{2c^2}\right] . \tag{56}$$

This gives

$$\mathrm{Re}[Z] = Z_o\zeta_{\mathrm{Re}}(\alpha) , \tag{57}$$

where

$$\zeta_{\mathrm{Re}}(\alpha) = \frac{1}{4\pi}\left\{1-(1+\alpha^2)\exp[\alpha^2]\Gamma(0,\alpha^2)\right\} , \tag{58}$$

the dimensionless parameter α is defined as

$$\alpha = \frac{\omega\sigma_\perp}{\gamma c} , \tag{59}$$

and

$$\Gamma(0,x) = \int_x^\infty \frac{dt}{t}\exp[-t] \tag{60}$$

and $Z_o = 4\pi/c$ indicates the free-space impedance. A plot of the universal function $\zeta_{\mathrm{Re}}(\alpha)$, that is the real part of the impedance in units of Z_o, is given in Fig. 3. Note that Re[Z] exhibits a singular behavior for $\sigma_\perp \longrightarrow 0$ (i.e. for $\alpha \longrightarrow 0$ in Fig. 3). This is linked with our particular model, where we chose $d_a \longrightarrow 0$.

4.2 Imaginary part

Since, in the limit for $z \gg \gamma^2 \lambda\!\!\!^{-}$, Z_2 is a real quantity, from Eq. (45) follows that the imaginary part of Z is

$$\mathrm{Im}[Z](\omega,z) = -\frac{\omega}{2\gamma^2}\,\mathrm{Im}\Bigg\{\int d\vec{r'}_\perp \int d\vec{r''}_\perp \rho_o^*(\vec{r'}_\perp)\rho_o(\vec{r''}_\perp) \times \int_0^z dz' \int_0^{z'} dz'' \frac{2i}{(z'-z'')}\exp\left[\frac{i\omega(z''-z')}{2\gamma^2 c} + i\omega\frac{|\,\vec{r'}_\perp - \vec{r''}_\perp\,|^2}{2c(z'-z'')}\right]\Bigg\}. \tag{61}$$

In the asymptotic limit for $z \gg 2\gamma^2 \lambda\!\!\!^{-}$ one finds the same result that one would have found calculating the impedance with the steady state expression for the field, Eq. (21), and substituting z_o with zero that is

$$\mathrm{Im}[Z](\omega,z) = -\frac{\omega}{2\gamma^2}\,\mathrm{Im}\Bigg\{\int d\vec{r'}_\perp \int d\vec{r''}_\perp \rho_o^*(\vec{r'}_\perp)\rho_o(\vec{r''}_\perp) \times \int_0^z dz' \int_0^{\infty} dz'' \frac{2i}{(z'-z'')}\exp\left[\frac{i\omega(z''-z')}{2\gamma^2 c} + i\omega\frac{|\,\vec{r'}_\perp - \vec{r''}_\perp\,|^2}{2c(z'-z'')}\right]\Bigg\}. \tag{62}$$

With the help of Eq. (19) we find the analogous of Eq. (51) for the imaginary part of the impedance in the asymptotic limit for $z \gg 2\gamma^2 \lambda\!\!\!^{-}$:

$$\mathrm{Im}[Z](\omega,z) = -\frac{2\omega z}{\gamma^2}\int d\vec{r'}_\perp \int d\vec{r''}_\perp \rho_o^*(\vec{r'}_\perp)\rho_o(\vec{r''}_\perp) K_o\left(\frac{\omega\,|\,\vec{r}_\perp - \vec{r'}_\perp\,|}{\gamma c}\right) \tag{63}$$

Similarly as for Eq. (47), we observe that the integral in $\vec{r''}_\perp$ can be interpreted as a convolution. In analogy with Eq. (48) we obtain

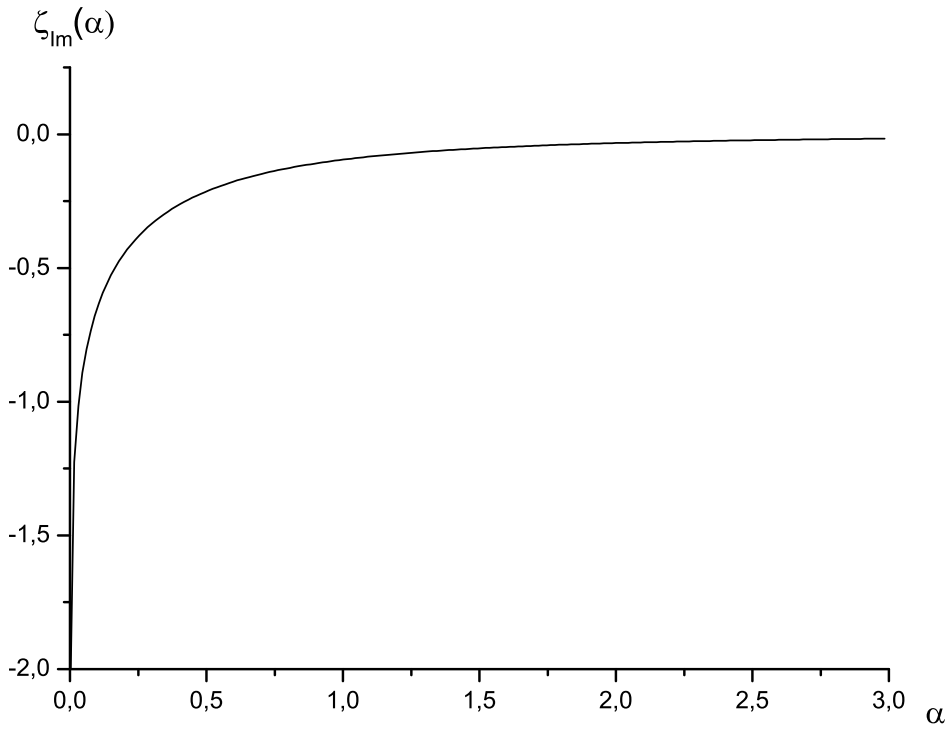

Fig. 4. Plot of the universal function ζ_{Im}, as a function of α.

$$\mathrm{Im}[Z](\omega, z) = -\frac{\omega z}{2\pi^2\gamma^2} \int d\vec{k} \left|\tilde{\rho}_o(\vec{k})\right|^2 \tilde{K}_o\left(\vec{k}\right) . \tag{64}$$

Finally, Eq. (54) together with the notation $\vec{\theta} = c\vec{k}/\omega$ yields

$$\mathrm{Im}[Z](\omega) = -\frac{1}{\pi}\omega z \int d\vec{\theta} \left|\tilde{\rho}_o(\vec{\theta}, \omega)\right|^2 \frac{1}{(1+\gamma^2\theta^2)} . \tag{65}$$

Similarly as for the real part, use of Eq. (56) allows to give an explicit expression for Im[Z]:

$$\mathrm{Im}[Z] = (Z_o\hat{z})\, \zeta_{\mathrm{Im}}(\alpha) , \tag{66}$$

where

$$\zeta_{\mathrm{Im}}(\alpha) = -\frac{1}{2\pi} \exp[\alpha^2]\, \Gamma(0, \alpha^2) , \tag{67}$$

the dimensionless parameter α is defined as in Eq. (59), Γ was given in Eq. (60), $Z_o = 4\pi/c$ indicates, as before, the free-space impedance, and $\hat{z} =$

$z/(2\gamma^2\lambda\!\!\!^{-})$. A plot of the universal function $\zeta_{\mathrm{Im}}(\alpha)$, that is the imaginary part of the impedance in units of $Z_o\hat{z}$ is given in Fig. 4.

Note that one may use different models for the electron beam transverse profile to be substituted in Eq. (65). For example, one may consider a stepped profile defined by

$$\rho_o(\vec{r}_\perp) = \frac{1}{\pi r_b^2 c}\, C_{r_b}(\vec{r}_\perp)\,, \tag{68}$$

where r_b is now the beam radius and $C_{r_b}(\vec{r}_\perp)$ is a circle function, equal to unity for $|\vec{r}_\perp| < r_b$ and zero otherwise. The analogous of Eq. (56) is

$$\tilde{\rho}_o(\vec{\theta},\omega) = \frac{2}{\omega r_b \theta} J_1\left(\frac{\omega r_b \theta}{c}\right)\,. \tag{69}$$

By substituting Eq. (69) in Eq. (65) and performing integration we recover the already known expression for the longitudinal space-charge impedance in case of a stepped profile bunch

$$Z_{LSC}(\omega) = -\frac{4icz}{\omega r_b^2}\left[1 - \frac{\omega r_b}{c\gamma} K_1\left(\frac{\omega r_b}{\gamma c}\right)\right], \tag{70}$$

in agreement with [14] where an expression per unit length is given, and the overall difference of a minus sign fixes the sign of the energy loss (using the convention in Eq. (70) it is negative).

5 Energy conservation

It is interesting to verify the energy conservation law for the active part of the field, that is Eq. (29).

With the help of Eq. (30), Eq. (43) and Eq. (55) we can immediately write the left hand side of Eq. (29) in its final form as

$$2\int_V \mathrm{Re}\left[\bar{j}_z^{\,*}\bar{E}_z\right]\, dV = -\frac{2c}{\pi}\left|\bar{f}(\omega)\right|^2 \int d\vec{\theta}\left|\tilde{\rho}_o(\vec{\theta},\omega)\right|^2 \frac{\gamma^4\theta^2}{\left(1+\gamma^2\theta^2\right)^2}\,. \tag{71}$$

We now need to calculate the right hand side of Eq. (29). This is the spectral energy density of radiation integrated over a transverse plane in the

far zone, i.e. at a large longitudinal distance z with respect to the radiation formation length $2\gamma^2\lambda\!\!\!^{-}$ at all wavelengths of interest, i.e. for $\lambda\!\!\!^{-} \gtrsim \sigma_z$. This gives $z \gg 2\gamma^2\sigma_z$, $2\gamma^2\sigma_z$ being the already-defined overtaking length. Radiation is generated because of the acceleration process, and is linked with the longitudinal wakes through Eq. (29). Radiation and longitudinal wakes should actually be seen as two faces of the same coin. We have already seen that major simplifications arise in the calculation of the impedance (and, therefore, of the wake) as one assumes a very short acceleration distance d_a compared with the overtaking length, $d_a \ll 2\gamma^2\sigma_z$. In particular, in this case, the impedance does not depend on the details of the acceleration process, that can be considered as taking place at a single point. This fact has its reflection on the characteristics of radiation, that are also bound to be independent of how acceleration took place, always provided that $d_a \ll 2\gamma^2\lambda\!\!\!^{-}$ at all wavelengths of interest. The acceleration process works as a switch in the space-frequency domain, in the sense that it switches on the harmonic contents of the electromagnetic sources at a given wavelength of interest. As long as it takes place within a distance much smaller than $2\gamma^2\lambda\!\!\!^{-}$, such switching process may have very different physical realizations. It may be due to an ultra-high field gradient, but also to a bending magnet deflecting an electron beam from an off-axis trajectory to a trajectory along the z axis, or to the crossing of an interface between two media with different dielectric properties. All these examples produce well-documented types of collimated radiation in the long wavelength range ($\lambda\!\!\!^{-} \gtrsim \sigma_z$). Radiation due to longitudinal acceleration is studied in [10], while if the switcher is a bend one obtains edge radiation (see [15] among many others, and references therein). Finally, passage through an interface between different media produces transition radiation. In particular, coherent transition radiation in the far zone generated at the interface between plasma and vacuum in a laser-plasma accelerator (with $d_a \ll 2\gamma^2\lambda\!\!\!^{-}$) has first been studied in [16]. Characteristics of these kinds of radiation coincide as long as the switching process obeys $d_a \ll 2\gamma^2\lambda\!\!\!^{-}$ [3].

In reference [17] we showed how radiation produced by a single ultrarelativistic electron can be suggestively described in terms of a laser-like beam. Once the waist of this laser beam is specified, the field distribution at any position down the z-axis can be found applying Fourier Optics techniques (in free-space this amounts to the application of Fourier propagation equation). In particular, a single electron created at $z_A = 0$ by the system depicted

[3] From this viewpoint, we do not agree with [16] about the presence of diffraction radiation when the electron beam is created inside the plasma. There is a principle difference between a case when an electron travels through a foil with finite transverse size and another when an electron is created at the interface between plasma and vacuum. When $d_a \ll 2\gamma^2\lambda\!\!\!^{-}$ radiation characteristics should not depend on the transverse characteristics of the plasma.

in Fig. 2 produces a laser-like beam is with a waist located at $z_A = 0$. As we have just discussed, since $d_a \ll 2\gamma^2 \lambda\!\!\!^{-}$, the field distribution at the waist does not depend on the realization of the accelerator setup, and coincides with that produced by a magnet edge, or by transition radiation. It is given by the field distribution associated with a single electron created at $z_A = 0$ and travelling along the z axis [17]:

$$\vec{\vec{E}}_{\perp s}(\vec{r}_\perp) = \frac{2i(-e)\omega}{c^2\gamma}\frac{\vec{r}_\perp}{r_\perp}K_1\left(\frac{\omega r_\perp}{c\gamma}\right) . \tag{72}$$

In our case though, we are considering an electron beam and not a single electron. This means that we are not dealing with a single laser-like beam but, rather, with a coherent collection of laser-like beams. At the initial point $z_A = 0$ each electron is completely characterized by an offset $\vec{r'}_\perp$ and a deflection angle $\vec{\phi'}_\perp$ with respect to the z axis. These two vectors identify a point in the transverse electron phase space. Each electron, characterized by the pair $(\vec{r'}_\perp, \vec{\phi'}_\perp)$, corresponds to a different laser-like beam, whose waist is simply tilted of an angle $\vec{\phi'}_\perp$ and shifted of an offset $\vec{r'}_\perp$. Accounting for offsets and deflections, Eq. (72) can be written as

$$\vec{\vec{E}}_{\perp s}(\vec{r}_\perp) = \frac{2i(-e)\omega}{c^2\gamma}\exp\left[i\frac{\omega}{c}\vec{\phi'}\cdot\left(\vec{r}_\perp - \vec{r'}_\perp\right)\right]\frac{\vec{r}_\perp - \vec{r'}_\perp}{\left|\vec{r}_\perp - \vec{r'}_\perp\right|}K_1\left(\frac{\omega\left|\vec{r}_\perp - \vec{r'}_\perp\right|}{c\gamma}\right) . \tag{73}$$

We now have to average Eq. (73) over the harmonic component of the charge density at frequency ω, i.e. $\bar{\rho}$ in Eq. (6) calculated at $z' = 0$, at the waist position. In principle, $\bar{\rho}$ should depend on both $\vec{\phi'}_\perp$ and $\vec{r'}_\perp$. However, in our model, it only depends on $\vec{r'}_\perp$, since we posed $\rho_o = \rho_o(\vec{r'}_\perp)$. In our situation of interest we can set $\vec{\phi'}_\perp = 0$ in Eq. (73) and obtain the following average over $\bar{\rho}$:

$$\vec{\vec{E}}_\perp(\vec{r}_\perp) = -\frac{2i\omega}{c^2\gamma}\bar{f}(\omega)\int d\vec{r'}_\perp \rho_o(\vec{r'}_\perp)\frac{\vec{r}_\perp - \vec{r'}_\perp}{\left|\vec{r}_\perp - \vec{r'}_\perp\right|}K_1\left(\frac{\omega\left|\vec{r}_\perp - \vec{r'}_\perp\right|}{c\gamma}\right) . \tag{74}$$

The right hand side of Eq. (29) in the space-frequency domain, is given by calculating the flux of the complex Poynting vector through the surface A_o (shown in Fig. 2). Such flux is equal to the flux of the complex Poynting vector associated with the virtual source through the virtual source, because the Fresnel propagator conserves the flux of the Poynting vector. Therefore the right hand side of Eq. (29) amounts to

$$-\frac{c}{2\pi}\int\limits_{A_o}\left|\vec{\vec{E}}_\perp\right|^2\,dA =$$

$$-\frac{c}{2\pi}\int d\vec{r}_\perp\left|\frac{2\omega}{c^2\gamma}\bar{f}(\omega)\int d\vec{r'}_\perp\rho_o(\vec{r'}_\perp)\frac{\vec{r}_\perp-\vec{r'}_\perp}{\left|\vec{r}_\perp-\vec{r'}_\perp\right|}K_1\left(\frac{\omega\left|\vec{r}_\perp-\vec{r'}_\perp\right|}{c\gamma}\right)\right|^2 . \qquad (75)$$

Note that the integral in $d\vec{r'}_\perp$ is a convolution product. As before, applying Eq. (40) with $g_1 = g_2$ to Eq. (75) and remembering that the spatial Fourier transform of the convolution product of two function is equal to the product of the spatial Fourier transform of the same functions, we can rewrite Eq. (75) as

$$-\frac{c}{2\pi}\int\limits_{A_o}\left|\vec{\vec{E}}_\perp\right|^2\,dA = -\frac{2\omega^2}{\pi c\gamma^2}\frac{1}{4\pi^2}\left|\bar{f}(\omega)\right|^2\int d\vec{k}\left|\tilde{\rho}_o(\vec{k})\tilde{\mathcal{F}}\left(\vec{k}\right)\right|^2 , \qquad (76)$$

where

$$\tilde{\mathcal{F}}\left(\vec{k}\right) = \int d\vec{r}_\perp\exp\left[i\vec{k}\cdot\vec{r}_\perp\right]\frac{\vec{r}_\perp}{r_\perp}K_1\left(\frac{\omega r_\perp}{c\gamma}\right) = \frac{2\pi\gamma^2c^2}{\omega^2}\frac{\gamma\theta}{1+\gamma^2\theta^2} , \qquad (77)$$

having used the notation $\theta = c/\omega\vec{k}$. Substituting Eq. (77) into Eq. (76) we obtain the final result

$$-\frac{c}{2\pi}\int\limits_{A_o}\left|\vec{\vec{E}}_\perp\right|^2\,dA = -\frac{2c}{\pi}\left|\bar{f}(\omega)\right|^2\int d\vec{\theta}\left|\tilde{\rho}_o(\vec{\theta},\omega)\right|^2\frac{\gamma^4\theta^2}{\left(1+\gamma^2\theta^2\right)^2} , \qquad (78)$$

that coincides with the left hand side in Eq. (71) thus verifying Eq. (29) as it must be.

6 Analytical asymptote of the wake function

The anti-Fourier transform of the impedance gives back the wake function, that in its turn allows one to calculate the energy change per particle averaged over the transverse beam coordinates.

Analytical results can be found starting with the asymptotic limit of the impedance for $z \gg \gamma^2\lambda$.

6.1 Symmetric part of the wake

The symmetric part of the wake function G_S can be found calculating

$$G_S(\Delta s) = \frac{1}{2\pi}\int_{-\infty}^{\infty} d\omega\ \mathrm{Re}[Z](\omega)\exp\left[-i\omega\left(\frac{\Delta s}{\beta c}\right)\right]\ . \tag{79}$$

With the help of Eq. (55) and Eq. (56) one can rewrite Eq. (79) as

$$G_S(\Delta s) = -\frac{1}{\pi c}\int_0^{\infty} d\theta \frac{\gamma^4\theta^3}{\left(1+\gamma^2\theta^2\right)^2}\int_{-\infty}^{\infty} d\omega\ \exp\left[-\frac{\theta^2\omega^2\sigma_\perp^2}{c^2}\right]\exp\left[-i\omega\left(\frac{\Delta s}{c}\right)\right]\ . \tag{80}$$

We first calculate the integral in $d\omega$, thus obtaining

$$G_S(\Delta s) = -\frac{1}{\sqrt{\pi}\sigma_\perp}\int_0^{\infty} d\theta \frac{\gamma^4\theta^2}{\left(1+\gamma^2\theta^2\right)^2}\exp\left[-\frac{(\Delta s)^2}{4\theta^2\sigma_\perp^2}\right]\ . \tag{81}$$

Performing the integral in $d\theta$ and using the notation $\Delta\xi = \gamma(\Delta s)/\sigma_\perp$ one obtains

$$G_S(\Delta\xi) = \frac{\gamma}{\sigma_\perp}H_S(\Delta\xi) \tag{82}$$

where

$$H_S(\Delta\xi) = -\frac{1}{4\sqrt{\pi}}\left\{\sqrt{\pi}\,|\Delta\xi| + \pi\left[1-\frac{(\Delta\xi)^2}{2}\right]\exp\left[\frac{(\Delta\xi)^2}{4}\right]\mathrm{erfc}\left[\frac{|\Delta\xi|}{2}\right]\right\}\ , \tag{83}$$

and

$$\mathrm{erfc}(x) = 1 - \frac{2}{\sqrt{\pi}}\int_0^x \exp[-t^2]dt\ . \tag{84}$$

A plot of the universal function H_S, that is the symmetric part of the wake in units of $\gamma/\sigma_\perp$, as a function of $\Delta\xi$ is given in Fig. 5.

Note that Eq. (82) can be verified in the asymptotic limit for $(\gamma\Delta s)^2 \gg \sigma_\perp^2$, i.e. $(\Delta\xi)^2 \gg 1$. If we further assume $(\Delta s)^2 \gg \sigma_z^2$ we obtain the asymptote

for two particles separated by a distance Δs. It may be useful to remind that in agreement with [11], the case of a test particle in front of the source corresponds to negative values of Δs. In this case, the longitudinal electron density distribution and its Fourier transform may be written respectively as

$$f(t) = (-e)\left[\delta\left(t - \frac{\Delta s}{2\beta c}\right) + \delta\left(t + \frac{\Delta s}{2\beta c}\right)\right] \tag{85}$$

and

$$f(\omega) = (-e)\left\{\exp\left[i\omega\frac{\Delta s}{2\beta c}\right] + \exp\left[-i\omega\frac{\Delta s}{2\beta c}\right]\right\} . \tag{86}$$

Substitution of Eq. (86) and Eq. (56) into Eq. (78) and use of Eq. (32) yields

$$\Delta\mathcal{E}_{\text{tot}} = \frac{2e^2}{\pi c}\int_{-\infty}^{\infty} d\omega \left\{1 + \cos\left[\frac{\omega(\Delta s)}{c}\right]\right\} \int_0^{\infty} d\theta \exp\left[-\frac{\theta^2\omega^2\sigma_\perp^2}{c^2}\right] \frac{\gamma^4\theta^3}{(1+\gamma^2\theta^2)^2}. \tag{87}$$

The first term in parenthesis {...} is related to single-particle radiation in the far zone, while the second term in cos(·) may be interpreted as the interference term between the field radiated by the two particles in the far zone. Let us consider the interference term alone, that will be indicated with $\Delta\mathcal{E}_{\text{int}}$. Performing first the integral in $d\omega$ we obtain

$$\Delta\mathcal{E}_{\text{int}} = \frac{2e^2}{\sqrt{\pi}\sigma_\perp}\int_0^{\infty} d\theta \exp\left[-\frac{(\Delta s)^2}{4\theta^2\sigma_\perp^2}\right] \frac{\gamma^4\theta^2}{(1+\gamma^2\theta^2)^2} . \tag{88}$$

In the limit for $(\gamma\Delta s)^2 \gg \sigma_\perp^2$, Eq. (88) can be written as

$$\Delta\mathcal{E}_{\text{int}} = \frac{2e^2}{\sqrt{\pi}\sigma_\perp}\int_0^{\infty} dx \exp\left[-\frac{x^2(\Delta s)^2}{4\sigma_\perp^2}\right] = \frac{2e^2}{\Delta s} , \tag{89}$$

where we have performed a change of integration variable to $x = 1/\theta$. The energy term $\Delta\mathcal{E}_{\text{int}}$ is due to the interaction between the two particles, and corresponds to the energy dissipated by the system through the active part of the wake.

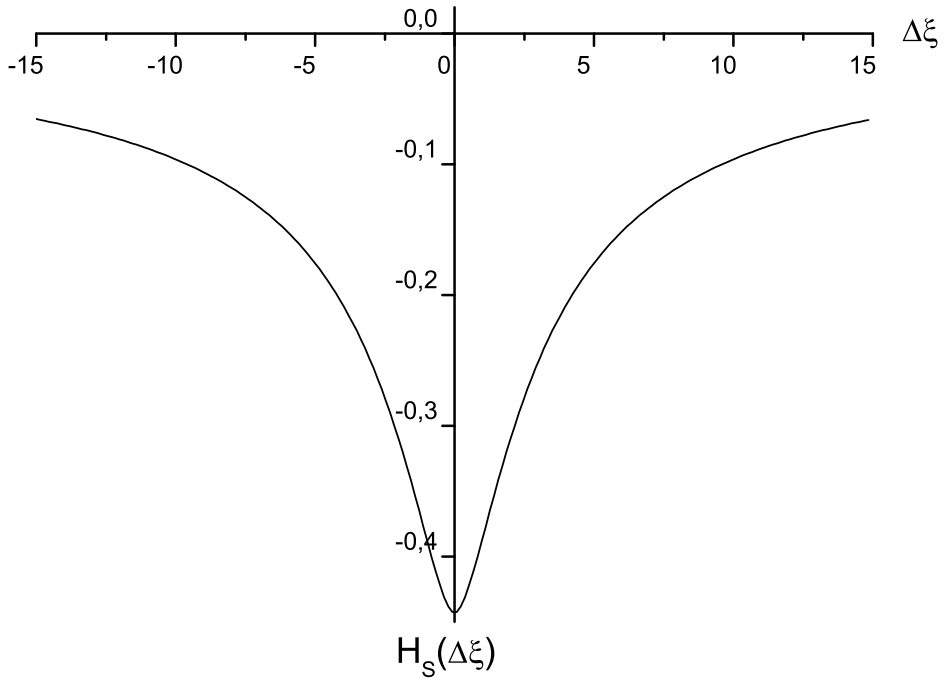

Fig. 5. Plot of the universal function H_S as a function of $\Delta\xi$.

Now, from Eq. (81) we have that the energy lost by one particle is $e^2 G_S(\Delta s) \longrightarrow -e^2/(\Delta s)$ when $(\gamma\Delta s)^2 \gg \sigma_\perp^2$. Since the system is composed by two electrons and the wake G_s is symmetric, the total energy lost by the system is given by twice this value. Thus, in the limit $(\gamma\Delta s)^2 \gg \sigma_\perp^2$, the energy dissipated by the system due to the active part of the wake is

$$2e^2 G_S(\Delta s) = -\frac{2e^2}{\Delta s}\,, \tag{90}$$

in agreement with Eq. (89), as it must be.

The energy gained or lost by a single particle at position s within the bunch due to the active (symmetric) part of the wake, averaged over transverse coordinates is given by

$$\Delta\mathcal{E}_S(s) = (-e)\int_{-\infty}^{\infty} G_S(\Delta s) f(s-\Delta s) d(\Delta s)\,. \tag{91}$$

Note that this expression can also be presented in terms of impedances as

$$\Delta\mathcal{E}_S(s) = \frac{1}{2\pi}\int_{-\infty}^{\infty} d\omega\ \mathrm{Re}[Z](\omega)\bar{f}(\omega)\exp\left[-i\omega\left(\frac{\Delta s}{\beta c}\right)\right], \tag{92}$$

which however appears not to yield any computational advantage over Eq. (91). Analogous remark holds for the antisymmetric part of the wake.

With the help of Eq. (12) and Eq. (82), we can explicitly write $\Delta\mathcal{E}_S/\mathcal{E}_o$, $\mathcal{E}_o = \gamma m_e c^2$ being the nominal energy of an electron (with rest mass m_e) as a function of $\xi = \gamma s/\sigma_\perp$:

$$\frac{\Delta\mathcal{E}_S}{\mathcal{E}_o}(\xi) = \frac{I_{\max}}{\gamma I_A}\int_{-\infty}^{\infty} d(\Delta\xi) H_S(\xi - \Delta\xi)\exp\left[-\frac{(\Delta\xi)^2}{2\eta^2}\right], \tag{93}$$

where we introduced the new parameter $\eta = \gamma\sigma_z/\sigma_\perp$, and we called the Alfven current $I_A = e/(mc^3) \simeq 17\,\mathrm{kA}$ and the beam current $I_{\max} = eNc/(\sqrt{2\pi}\,\sigma_z)$.

From a methodological point of view it is interesting to conclude our treatment of the symmetric part of the wake with an additional remark. On the one hand we have found that electrons in the bunch lose energy under the action of radiative interaction forces within an overtaking length $\sim 2\gamma^2\sigma_z$ *after* the accelerator. On the other hand, an observer in the far zone detecting the radiation pulse may calculate the retarded position of radiators, concluding that electrons radiated *inside* the accelerator. Methodological questions of this kind (electrons radiating when the radiative force does not work on them and vice versa) are related with other well-known situations of interest. For example, they also arise in Coherent Synchrotron Radiation (CSR) from bending magnets and were discussed in [18].

6.2 Antisymmetric part of the wake

The antisymmetric part of the wake function G_S can be found calculating

$$G_A(\Delta s) = \frac{i}{2\pi}\int_{-\infty}^{\infty} d\omega\ \mathrm{Im}[Z](\omega)\exp\left[-i\omega\left(\frac{\Delta s}{\beta c}\right)\right]. \tag{94}$$

With the help of Eq. (65) and Eq. (56) one can rewrite Eq. (94) as

$$G_A(\Delta s) = -\frac{iz}{\pi c^2}\int_0^\infty \frac{d\theta\,\theta}{1+\gamma^2\theta^2}\int_{-\infty}^\infty d\omega\,\omega \exp\left[-\frac{\theta^2\omega^2\sigma_\perp^2}{c^2}\right]\exp\left[-i\omega\left(\frac{\Delta s}{c}\right)\right] \quad .(95)$$

Using the fact that

$$\int_{-\infty}^\infty d\omega\,\omega \exp\left[-\frac{\theta^2\omega^2\sigma_\perp^2}{c^2}\right]\exp\left[-i\omega\left(\frac{\Delta s}{c}\right)\right] =$$
$$ic\frac{d}{d(\Delta s)}\int_{-\infty}^\infty d\omega\ \exp\left[-\frac{\theta^2\omega^2\sigma_\perp^2}{c^2} - i\omega\left(\frac{\Delta s}{c}\right)\right] = -\frac{i\sqrt{\pi}\,c^2\Delta s}{2\theta^3\sigma_\perp^3}\exp\left[-\frac{(\Delta s)^2}{4\theta^2\sigma_\perp^2}\right], \quad (96)$$

one obtains

$$G_A(\Delta s) = -\frac{z\,\Delta s}{2\sqrt{\pi}\sigma_\perp^3}\int_0^\infty \frac{d\theta}{(1+\gamma^2\theta^2)\theta^2}\exp\left[-\frac{(\Delta s)^2}{4\theta^2\sigma_\perp^2}\right]. \quad (97)$$

Performing the integral in $d\theta$ and using, as before, the notation $\Delta\xi = \gamma(\Delta s)/\sigma_\perp$ one has

$$G_A(\Delta\xi) = \frac{\gamma\eta\hat{z}}{\sigma_\perp}H_A(\Delta\xi) \quad (98)$$

where

$$H_A(\Delta\xi) = -\frac{1}{2\sqrt{\pi}}(\Delta\xi)\left\{2\frac{\sqrt{\pi}}{|\Delta\xi|} - \pi\exp\left[\frac{(\Delta\xi)^2}{4}\right]\mathrm{erfc}\left[\frac{|\Delta\xi|}{2}\right]\right\}, \quad (99)$$

and we redefined $\hat{z} = z/(2\gamma^2\sigma_z)$. A plot of the universal function H_A, that is the symmetric part of the wake in units of $\gamma\hat{z}/\sigma_\perp$, as a function of $\Delta\xi$ is given in Fig. 6.

Note that Eq. (98) can be verified in the asymptotic limit $(\gamma\Delta s)^2 \gg \sigma_\perp^2$, i.e. $(\Delta\xi)^2 \gg 1$. If we further assume $(\Delta s)^2 \gg \sigma_z^2$ we obtain the asymptote for two particles separated by a distance Δs as before for the symmetric part of the wake. $\Delta s < 0$ indicates again the case when the test particle is in front of the source. From the Lienard-Wiechert expression for the electric field of a single particle moving on a straight line we can calculate the rate of energy

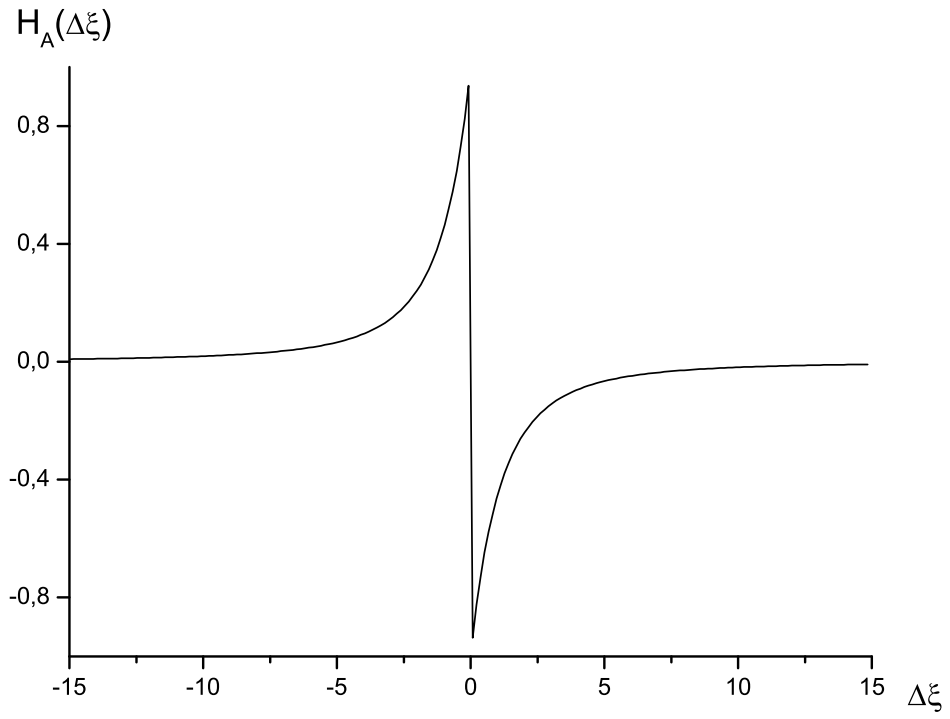

Fig. 6. Plot of the universal function H_A as a function of $\Delta\xi$.

change of the front electron

$$\frac{d\mathcal{E}}{dz} = \frac{e^2}{\gamma^2(\Delta s)^2} \,. \tag{100}$$

Independently, from Eq. (98) we have that $H_A(\Delta\xi) \longrightarrow -2\ \mathrm{sign}(\Delta\xi)/(\Delta\xi)^2$ when $(\Delta\xi)^2 \gg 1$. As a result, at position z the front particle has gained the energy

$$\Delta\mathcal{E}_A = e^2 G_A(\Delta s) = \frac{e^2 z}{\gamma^2(\Delta s)^2} \tag{101}$$

that corresponds to the rate of energy change in Eq. (100) as it must be.

The energy gained or lost by a single particle at position s within the bunch due to the reactive part of the wake, averaged over transverse coordinates is given by

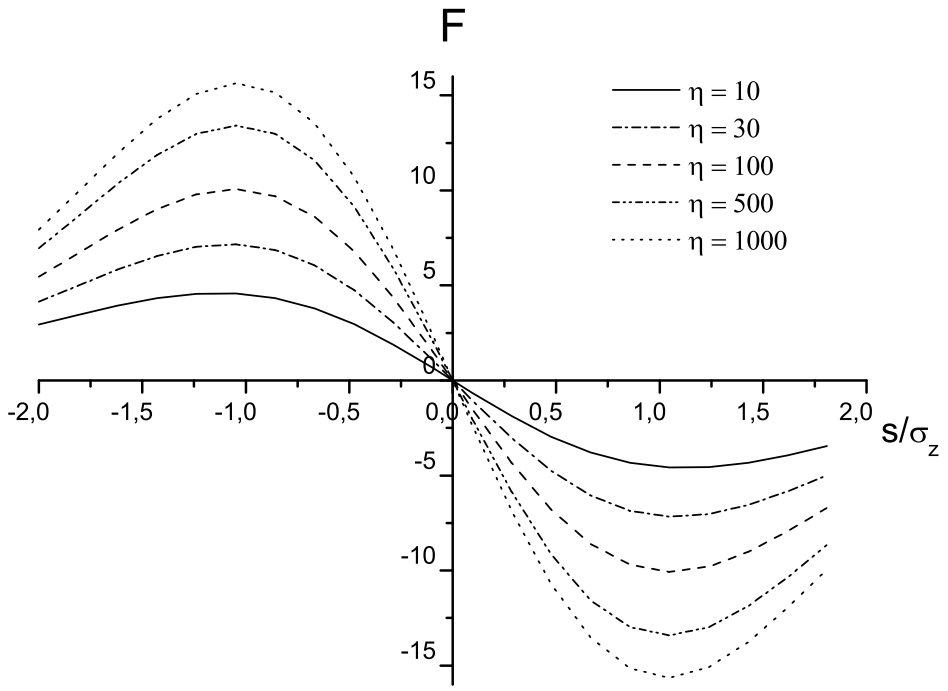

Fig. 7. Plot of F in Eq. (105) as a function of s/σ_z for different values of η.

$$\Delta\mathcal{E}_A(s) = (-e)\int_{-\infty}^{\infty} G_A(\Delta s) f(s-\Delta s) d(\Delta s)\,. \tag{102}$$

With the help of Eq. (12) and Eq. (98), we can explicitly write $\Delta\mathcal{E}_A/\mathcal{E}_o$, $\mathcal{E}_o = \gamma m_e c^2$ being the nominal energy of an electron (with rest mass m_e) as a function of $\xi = \gamma s/\sigma_\perp$:

$$\frac{\Delta\mathcal{E}_A}{\mathcal{E}_o}(\xi) = \frac{I_{\max}}{\gamma I_A}\,\eta\hat{z}\int_{-\infty}^{\infty} d(\Delta\xi) H_A(\xi-\Delta\xi)\exp\left[-\frac{(\Delta\xi)^2}{2\eta^2}\right]\,. \tag{103}$$

Note that Eq. (103) is a function of ξ but also depends parametrically on η, and may be presented as

$$\frac{\Delta\mathcal{E}_A}{\mathcal{E}_o}\left(\frac{s}{\sigma_z};\eta\right) = \frac{I_{\max}\hat{z}}{\gamma I_A} F\left(\frac{s}{\sigma_z};\eta\right)\,. \tag{104}$$

where we indicated the parametric dependence of η after the semicolon and

$$F\left(\frac{s}{\sigma_z};\eta\right)=\int_{-\infty}^{\infty} d(\Delta\xi)\,\eta\,H_A\left(\eta\frac{s}{\sigma_z}-\Delta\xi\right)\exp\left[-\frac{(\Delta\xi)^2}{2\eta^2}\right]\,. \tag{105}$$

A plot of Eq. (105) is given as a function of s/σ_z in Fig. 7 for different values of η.

We failed to integrate Eq. (93) and Eq. (103) (or Eq. (104)) analytically. However, plots for $\Delta\mathcal{E}_S/\mathcal{E}_o$ and $\Delta\mathcal{E}_A/\mathcal{E}_o$ as a function of ξ can be computed with the help of numerical techniques. In the following Section we will give a practical example of application of our work.

7 Impact on the design of a table-top FEL in the VUV and X-ray range

The foreseen specifications of the next generation laser-plasma accelerators are stunning. The high acceleration gradient will be up to TV/m, producing very short bunches about 10 fs long in the 100 kA current class (i.e. with a charge of about 1 nC). The beam quality is also expected to rival state-of-the art conventional acceleration techniques, featuring a relative energy spread of 0.1% for beam energies in the GeV range and a normalized emittance in the order of 1 mm·mrad.

One of the obvious and perhaps most exciting applications envisaged for these machines is as drivers for table-top FELs, both in the VUV (TT-VUV FEL) and in the X-ray range (TT-XFEL) [19]. Estimation of basic scaling parameters for Self-Amplified Spontaneous Emission (SASE) FEL applications within the one-dimensional ideal case indicate that a system composed by a laser-plasma accelerator and a meter-long undulator may undergo SASE process in the sub-nanometer range, thus outclassing all existing and foreseen XFEL projects, both in dimensions and costs.

Unfortunately, the road map towards the practical realization of this ambitious goal is not problem-free. Let aside other possible problems we focus our attention on a fundamental issue that, in our understanding, constitutes a serious difficulty. Namely, we want to estimate the impact of the longitudinal wake on the electron beam quality using the theory developed in the previous Sections. This is possible, because the plasma acceleration gradient is such that the electron beam to be injected in the undulator can be produced within distances $d_a \ll 2\gamma^2\sigma_z$, i.e. well within the applicability region of our theory. Note that our estimation is completely independent of the physical realization of the accelerator (a laser-plasma device, or any other physical principle). Within our model, the accelerator is just located at a single point at position z_A down the beamline.

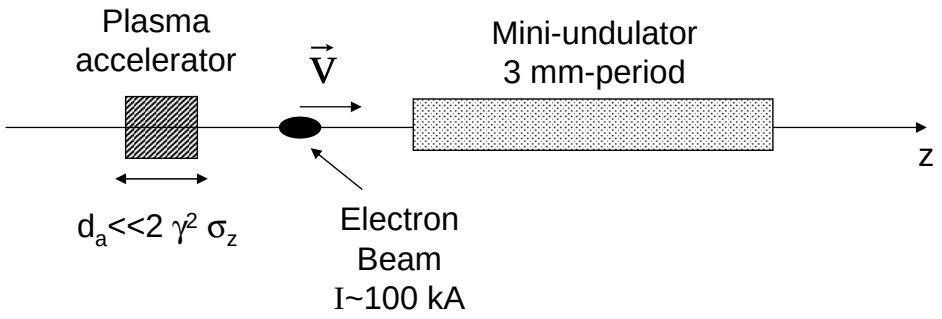

Fig. 8. Geometry of the TT-VUV FEL and of the TT-XFEL setups.

In the following we will consider two sets of parameters informally under discussion within the scientific community. The first refers to a test case designed to radiate in the VUV range ($\lambda = 25$ nm) while the second deals with the true table-top SASE XFEL, designed to radiate in the hard X-ray range ($\lambda = 0.25$ nm). Both parameter sets rely on the use of a mini-undulator with a 3 mm-period, that would allow low electron beam energy (in the order 100 MeV and 1 GeV for the VUV and the X-ray case). Very high currents, in the order of 100 kA, are supposed to be used . The geometry of the system is described in Fig. 8. It is important to note that in both study-cases the undulator parameter $K \simeq 0.5$. This means that the longitudinal velocity of particles in the undulator is not significatively altered ($\gamma_z^2 \equiv \gamma^2/(1 + K^2/2) \simeq 1.125\gamma^2$). As a result, wake field calculations in vacuum, performed in the preceding Sections, can still be used inside the undulator.

Description of the FEL setups will be limited to the one-dimensional model. In this case, the basic scaling parameter is the one-dimensional ρ_{1D} parameter defined as [20]

$$\rho_{1D} = \frac{\lambda_w}{4\pi}\left[\frac{2\pi^2 j_o K^2 A_{JJ}^2}{I_A \lambda_w \gamma^3}\right]^{1/3} \tag{106}$$

where j_o is the beam current density, λ_w is the undulator period, K is the undulator parameter defined as $K = e\lambda_w H_w/(2\pi m_e c^2)$, where H_w is the maximum magnetic field produced by the undulator on the z axis. Finally, the coupling factor A_{JJ}, for a planar undulator, is given by $A_{JJ} = J_0(Q) - J_1(Q)$, where $Q = K^2/(2 + K^2)$. The main quantities of interest characterizing the FEL process can be written in terms of ρ_{1D}. In fact, the one-dimensional power gain length of a mono-energetic beam is

$$L_G = \frac{\lambda_w}{4\pi\sqrt{3}\rho_{1D}}\,, \tag{107}$$

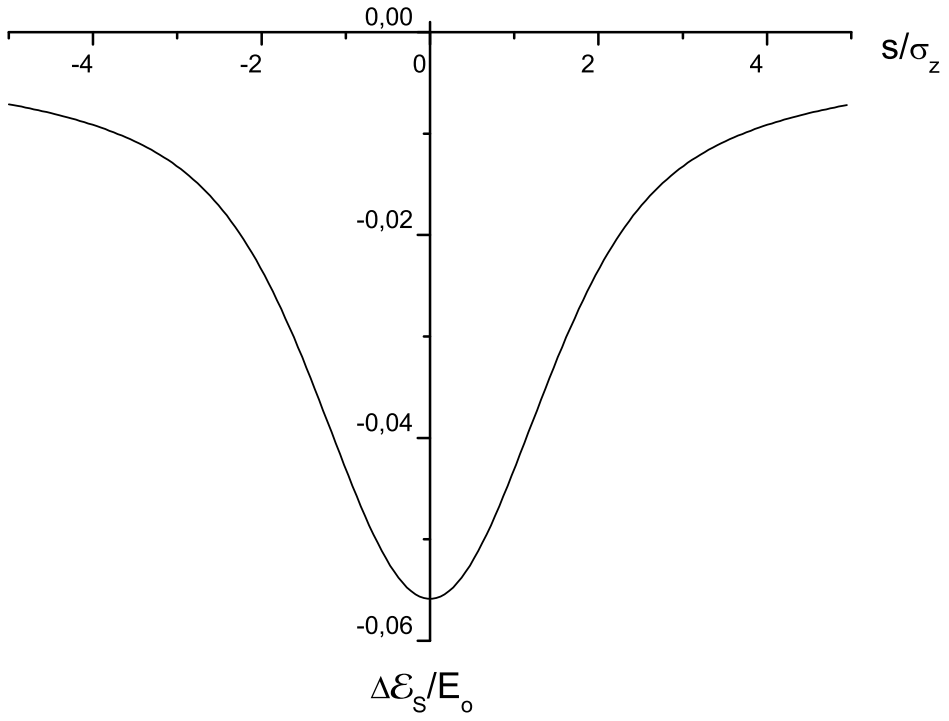

Fig. 9. Relative energy change $\Delta\mathcal{E}_s/\mathcal{E}_o$ as a function of the position inside the bunch s/σ_s in the case of the VUV table top FEL setup.

while the relative FEL bandwidth at saturation is close to ρ_{1D} and the power at saturation is about ρ_{1D} times the electron beam power.

Let us first deal with the VUV test case, that aims at producing radiation at a wavelength $\lambda = 25$ nm using an electron energy $\mathcal{E}_o = 130$ MeV and a 0.7 m-long undulator with period $\lambda_w = 3$ mm. The electron beam current is about 60 kA. The longitudinal beam size is taken to be $\sigma_z \sim 1$ μm. The transverse beam dimension is changed, instead, from an initial size $\sigma_\perp = 1$ μm to a final size $\sigma_\perp \sim 30$ μm within a few centimeters. In our estimation we will neglect the impact of this change of dimension on the longitudinal wake, and take $\sigma_\perp \sim 30$ μm from the very beginning.

The radiation formation length at wavelength λ is estimated to be $2\gamma^2\lambda\!\!\!^{-}$, and our asymptotic calculations for the impedance are valid for $z \gg 2\gamma^2\lambda\!\!\!^{-}$. An estimation of the wavelengths of interest is given considering the typical length scale that enters in the expressions for the impedance. In our case we take $\lambda\!\!\!^{-} \simeq \sigma_z = 1$ μm, which yields $2\gamma^2\lambda\!\!\!^{-} \simeq 10$ cm, a few times smaller than the size of the TT-VUV FEL, because the planned length of the undulator is about 0.7 m. This allows us to use asymptotic expressions Eq. (93) and Eq. (103). The only parameters needed to be plugged into these equations are

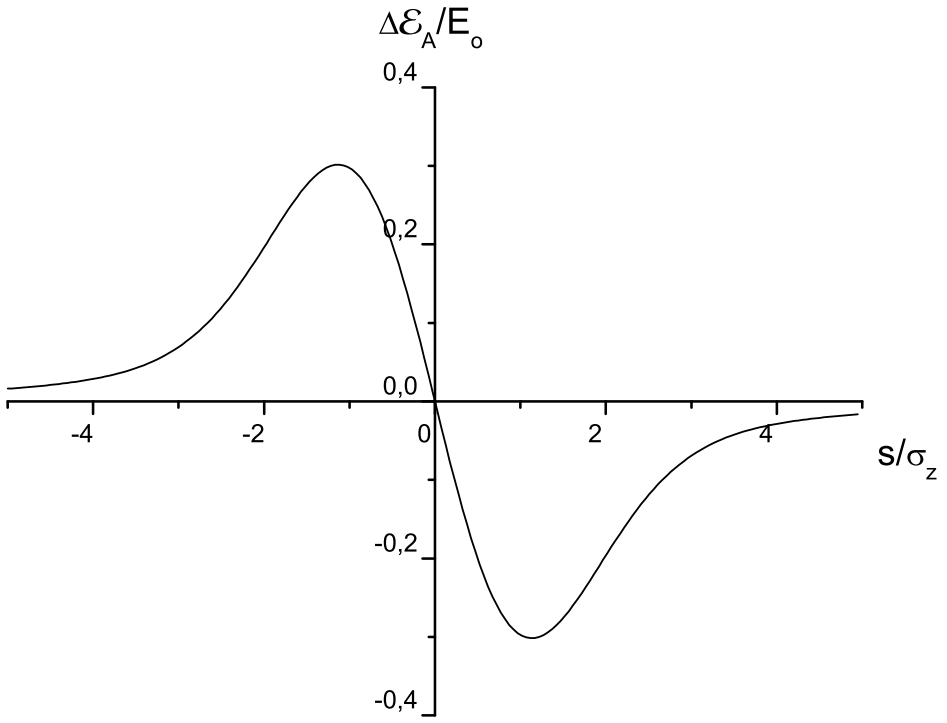

Fig. 10. Relative energy change $\Delta\mathcal{E}_A/\mathcal{E}_o$ as a function of the position inside the bunch s/σ_s in the case of the VUV table top FEL setup. This plot refers to the position $z = 0.7$ m.

thus $\gamma = 260$ and $\eta = 8.7$ and $I = 60$ kA. Moreover, since the asymmetric part of the wake is proportional to $\hat{z} = z/(2\gamma^2\sigma_z)$, we need to fix a position along the longitudinal axis to calculate Eq. (103). Here we set $z \simeq 0.7$ m, corresponding to the foreseen undulator length. The relative energy change $\Delta\mathcal{E}_{S,A}/\mathcal{E}_o$ calculated with the help of Eq. (93) and Eq. (103) is plot respectively in Fig. 9 and Fig. 10 as a function of the longitudinal coordinate inside the bunch. While travelling down the undulator, a correlated energy change develops along the electron beam. In our case the chirp is non-linear, but in order to estimate the magnitude of the effect we can use the linear energy chirp parameter [21, 22]:

$$\hat{\alpha} = -\frac{d\gamma}{dt}\frac{1}{\gamma\omega\rho_{1D}^2}\,. \tag{108}$$

The effect of linear energy chirp starts to play a significant role on the FEL gain when $\hat{\alpha} \gtrsim 1$. Intuitively, this means that the relative energy change becomes comparable with the FEL parameter on the scale of the coherence length. Using an estimation of the slope around $s = 0$ in Fig. 10 and the

other problem parameters one finds $\hat{\alpha} \simeq 12$, that indicates a very large effect. It is important to note that in our case the energy chirp in Fig. 10 depends on the electron beam profile but also on time, because it develops along the undulator. This effect is fundamental, it cannot be avoided, and is directly linked with the feasibility of the proposed FEL scheme. In other words, radiation generated in one part of the undulator cannot interact in resonance in another part of the undulator, and the amplification process is destroyed.

In these conditions, our conclusion is that the proposed TT-VUV FEL setup will not work.

Let us now turn to consider a table-top SASE XFEL scenario aimed at producing radiation at a wavelength $\lambda = 0.25$ nm using an electron energy $\mathcal{E}_o = 1.2$ GeV and a 3m-long undulator with period $\lambda_w = 3$ mm. The electron beam current is taken in the 100 kA range. We take again $\sigma_z = 1$ μm, and $\sigma_\perp = 30$ μm. Similarly as before we estimate the radiation formation length taking $\lambda\!\!\!^{-} \simeq \sigma_z$. This yields $2\gamma^2\lambda\!\!\!^{-} \simeq 10$ m, longer than the TT-XFEL undulator length, that is about 3 m. This makes it impossible to use our asymptotic expressions, Eq. (93) and Eq. (103), because the entire setup is well within the formation length. This situation needs further study, based on detailed numerical simulations, that goes beyond the scope of this work. However, as before, we can say that longitudinal wake fields will be responsible for an energy chirp that is both profile dependent and time dependent. Moreover, even though the electron beam energy has increased of an order of magnitude (thus leading to a decrease of the energy change level), the ρ_{1D} parameter is decreased of an order of magnitude. Since the undulator length is only a factor three shorter than the formation length, we conclude that wake fields constitute a major effect in this case too. Such effect poses a serious threat to the operation of the TT-XFEL setup.

8 Conclusions

This work constitutes the first study of the impact of longitudinal wake fields on the quality of electron beams produced with high field-gradient accelerators. We restricted our attention to the analysis of the wake generated along the trajectory following the acceleration, and assuming that the acceleration happens on a short longitudinal scale compared with the overtaking length, i.e. $d_a \ll 2\gamma^2\sigma_z$. Thus, our consideration does not depend on the particular realization of the accelerator. However, given present technological developments, one of the most relevant applications of our study should come from the realm of laser-plasma accelerators.

We calculated longitudinal symmetric and anti-symmetric parts of the wake function as well as real and imaginary part of the impedance with the help of paraxial approximation within a space-frequency domain formulation of Maxwell's equation. While the general expressions for wakes and impedances need numerical techniques to be evaluated, it is possible to present analytical expressions for the asymptotic limit when the electron bunch has reached a position, down the beamline, that is far from the acceleration point, with respect to the overtaking distance. It should be noted that in these cases the wake and the impedance are proportional to universal functions, valid for any set of parameters.

Our results can be used as analytical benchmarks for computer codes. Moreover, the the asymptotic result for the antisymmetric part of the wake is of fundamental importance, in the sense that its validity is not restricted to the particular model studied in this paper (fast acceleration). To the best of our knowledge, Eq. (98) constitutes the first analytical solution to the problem of space-charge wakes (calculated per unit length). Taking advantage of similarity techniques we presented such result in terms of a dimensionless object dependent on the problem parameters ($\gamma\eta\hat{z}/\sigma_\perp$) multiplied by a universal function H_A (see Eq. (99)). Eq. (98) can further be used to calculate the relative energy change of a particle within a given bunch. In case of a Gaussian longitudinal profile the relative energy spread reduces to Eq. (104). Plots presented in Fig. 7 will help the reader to perform a fast estimation of the influence of the space-charge wake at the stage of planning of experiments.

As a particular example, we used our results to estimate the impact of the longitudinal wake fields on the energy change of the electron beam in a table top FEL setup, both in the VUV range (λ = 25 nm) and in the x-ray range (λ = 0.25 nm). In both situations, such energy variation is time and shape dependent. This effect is fundamental, in the sense that it cannot be avoided. The total energy deviation is found to be an important effect, and constitute a major problem for the exploitation of the SASE amplification process.

9 Acknowledgements

We thank Massimo Altarelli and Martin Dohlus (DESY) for many useful discussions, Reinhard Brinkmann and Jochen Schneider (DESY) for their interest in this work.

References

[1] S.P.D. Mangles et al., Nature 431, 535 (2004)
[2] C.G.R. Geddes et al., Nature 431, 538 (2004)
[3] J. Faure et al., Nature 431, 538 (2004)
[4] A.M. Kondratenko and E.L. Saldin, Part. Accelerators 10, 207 (1980)
[5] Ya. S. Derbenev, A.M. Kondratenko and E.L. Saldin, Nucl. Instrum. and Meth. in Phys. Res. 193, 415 (1982)
[6] J.B. Murphy and C. Pellegrini, Nucl. Instrum. and Meth. in Phys. Res. A 237, 159 (1985)
[7] V. Ayvazyan et al., Eur. Phys. J. D 37, 297 (2006)
[8] M. Altarelli et al. (Eds.), XFEL: The European X-Ray Free-Electron Laser. Technical Design Report, DESY 2006-097, DESY, Hamburg (2006) (See also http://xfel.desy.de)
[9] J. Arthur et al. Linac Coherent Light Source (LCLS). COnceptual Design Report, SLAC-R593, Stanford (2002) (See also http://www-ssrl.slac.stanford.edu/lcls/cdr)
[10] J. Jackson, "Classical Electrodynamics", 3rd ed., Wiley, New York (1999)
[11] B. Zotter and S. Kheifets, "Impedances and Wakes in High-Energy Particle Accelerators", World Scientific, Singapore, 1997
[12] H. Kramers, Atti Congr. Internaz. Fisici, Com, 2, pp. 545 (1927)
[13] R. Kronig and H. Kramers, Z. Phys., 52, 174 (1928)
[14] Z. Huang and T. Shaftan, Instrum. and Meth. in Phys. Res. A 528, 345 (2004)
[15] R.A. Bosch, Il Nuovo Cimento, 20, 4 p. 483 (1998)
[16] C.B. Schroeder, E. Esarey, J. van Tilburg and W. P. Leemans, Phys. Rev. E 69, 016501 (2004)
[17] G. Geloni, E. Saldin, E. Schneidmiller and M. Yurkov, "Fourier Optics Treatment of Classical Relativistic Electrodynamics", DESY 06-127 (2006)
[18] E.L. Saldin, E.A. Schneidmiller and M.V. Yurkov, Nucl. Instrum. and Meth. in Phys. Res. A 398, 373 (1997)
[19] F. Gruener et al. "Design Considerations of table-top FELs", in Proceedings of the 37th ICFA Beam Dynamics Workshop, Future Light Sources DESY, Hamburg, Germany (2006), see http://adweb.desy.de/mpy/FLS2006/proceedings/TALKS/PLT04_TALK.PDF
[20] R. Bonifacio, C. Pellegrini and L. Narducci, Opt. Commun. 50, 373 (1984)
[21] S. Krinsky and Z. Huang, Phys. Rev. ST Accel. Beams 6, 050702 (2006)
[22] E. L. Saldin, E. A. Schneidmiller, and M. V. Yurkov Phys. Rev. ST Accel. Beams 9, 050702 (2006)